LOW ENERGY PION PRODUCTION BY PROTONS WITH INCIDENT ENERGIES FROM 400 TO 500 MeV

by

EDWARD LAWRENCE MATHIE

B.Sc., University of Victoria, 1974

A THESIS SUBMITTED IN PARTIAL FULFILLMENT

OF THE REQUIREMENTS FOR THE DEGREE OF

MASTER OF SCIENCE

in the department

of

Physics

ACCEPTED

FACULTY OF GRADUATE STUDIES

[redacted]

Dean

DATE Sept 14, 1976

We accept this thesis as conforming

to the required standard

[redacted]

University of Victoria

May 1976

ABSTRACT

Supervisor: Professor G.A.Beer

The differential cross sections for production of positive pions by bombarding carbon with 400, 450 and 500 MeV protons and copper with 450 and 500 MeV protons have been measured. This data was taken at pion production angles of 60°, 100°, and 150° with respect to the incident proton beam.

The results are compared to theoretical calculations and to similar work at other proton energies. The earlier results of Lillethun at 450 MeV should be renormalized by a factor of approximately 0.3. As proton energy increases from 400 to 730 MeV the differential cross sections for a particular energy pion increase monotonically.

TABLE OF CONTENTS

LIST OF TABLES

LIST OF FIGURES

ACKNOWLEDGEMENTS

The author would like to thank Dr.G.A.Beer for assistance during 1974 and 1975, and Drs. L.P.Robertson and G.R.Mason for their supervision during the bulk of the pion production experiment. The author would also like to thank Drs. D.A.Bryman, A.Olin and J.S.Vincent for their assistance and patience throughout the experiment.

At all times the beam physicists at TRIUMF worked hard to improve the quality of the beam, however particular thanks are due Dr.E.W.Blackmore for his effort to provide six different proton energies during a single night shift.

For reading preliminary drafts of the thesis and offering many valuable comments, the author is indebted to Drs.R.M.Pearce, G.W.Bushnell and C.E.Picciotto.

Financial support from the University of Victoria and TRIUMF is gratefully acknowledged.

CHAPTER 1

INTRODUCTION

Pion production cross sections are important for several reasons. The differential cross sections may be used to choose the angle at which a secondary channel in a meson factory is located in order to maximize the flux of a specific energy range of pions. Estimates of these figures have been made on the basis of higher energy data for use in designing TRIUMF meson channels and data at TRIUMF energies is of immediate interest to evaluate the operation of these channels and the design of new channels. Pion production measurements provide a test of nuclear pion production models. Beder and Bendix (1971) have requested large angle data for this purpose.

Measurements have been made by James (1975) at proton energy 580 MeV and by Cochran et al (1972) at 730 MeV for a wide variety in targets and a wide range in the angles at which the pion is emitted. Hirt et al (1969) have measured pion production by 600 MeV protons at angles 0.8° and 21.5° with respect to the proton beam. Earlier measurements were made by Lillethun (1962) at 450 MeV, by Meshkovskii et al (1958) at 660 MeV, and by Haddock et al (1964) at 725 MeV. The latter two experiments were primarily concerned with high energy pions.

The purpose of this experiment was to measure low energy positive pion production differential cross sections at large angles with respect to an incident proton beam.

The measurements were intended to supplement those for proton energies 580 and 730 MeV for carbon and copper nuclei, with data between 400 and 500 MeV. Of particular interest was a measurement of the cross sections at 450 MeV, where Lillethun's data has been questioned by Hirt et al (1969), Beder and Bendix (1971), and James (1975).

The experimental technique is described in Chapter 2. Chapter 3 is a summary of the calculations of differential cross sections, $d^2\sigma/dT_\pi d\Omega$. An important calibration and check of the calculations was done by measuring pions produced in the two body reaction, $p(p,\pi)D$. This measurement and comparison with previous results is discussed in Chapter 4. The cross sections for nuclear pion production from carbon and copper are summarized and compared with similar cases and theoretical calculations in Chapter 5. Concluding remarks and a summary of this thesis are found in Chapter 6.

CHAPTER 2

EXPERIMENTAL TECHNIQUE

2.1 Pion Detection

To measure $d^2\sigma/dT_\pi d\Omega$ for pions the experimental method must allow separation of different energy pions at each production angle. A range telescope, shown in Fig.2.1, can be used to select particles of a given energy by placing the appropriate amount of absorber material between the source and the stopping counter number S_4. The logic coincidence signal for a particle stopping in counter S_4 is $1{\cdot}2{\cdot}3{\cdot}4{\cdot}\bar{5}$ which is defined to be a "STOP". The symbol $\bar{5}$ means no signal observed in counter S_5. For a particular thickness of absorber several types of particles with different energies may be stopped. To distinguish between the different types of particles, analog signals representing the time of flight between two counters and the energy lost in a third counter are digitized and recorded in two dimensional histograms. An example of the different mean stopping energies, energy losses and times of flight in the range telescope used is given in Table 2.1. From this example it is clear that protons can be separated from pions and muons, however time of flight and energy loss alone are not sufficient to separate pions and muons, and additional timing restraints based on the natural decays of the π^+ and μ^+ are invoked as described below.

The pion to muon decay, $\pi^+ \rightarrow \mu^+ + \upsilon_\mu$, has a mean lifetime

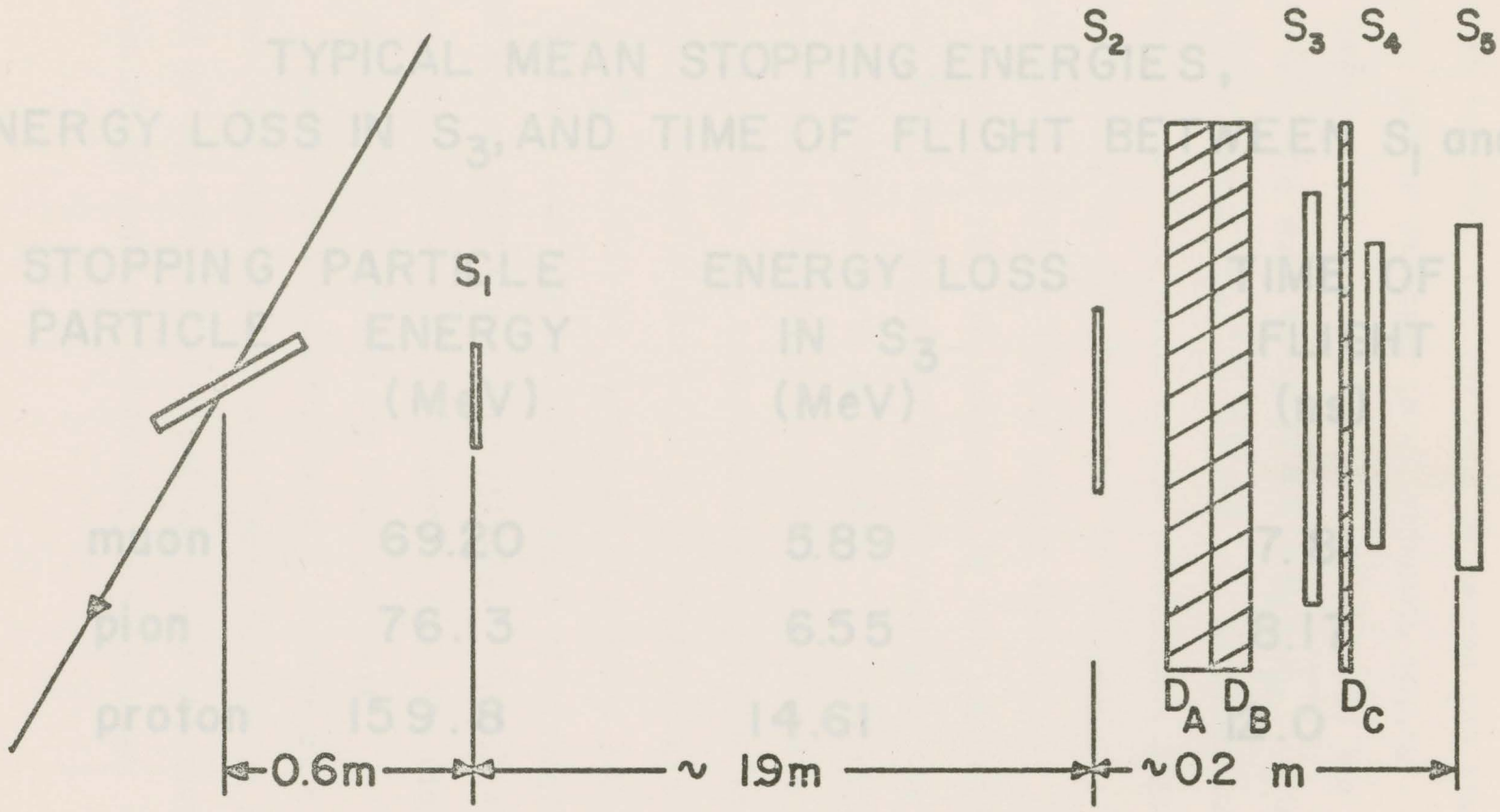

Fig.2.1 Schematic diagram of the range telescope showing target, counters and copper absorbers.

TABLE 2.1

TYPICAL MEAN STOPPING ENERGIES,
ENERGY LOSS IN S_3, AND TIME OF FLIGHT BETWEEN S_1 and S_2

STOPPING PARTICLE	PARTICLE ENERGY (MeV)	ENERGY LOSS IN S_3 (MeV)	TIME OF FLIGHT (ns)
muon	69.20	5.89	7.81
pion	76.13	6.55	8.17
proton	159.8	14.61	12.0

of $\tau_\pi = 26.0 ns$. The decay muon has a kinetic energy of 4.1 MeV when the pion decays at rest, which is in general too small for the muon to escape the stopping counter and be detected in an adjacent counter. A 4.1 MeV muon can travel approximately 1.6 mm in the counter material. The muon decay, $\mu^+ \rightarrow e^+ + \nu_e + \overline{\nu_\mu}$, has a mean lifetime of $\tau_\mu = 2.20 \mu s$. In order to separate stopped pions from muons in the telescope a signal corresponding to the pion decay in the stopping counter, S_4, is required within a 100 ns period following a STOP signal. Thus a stopped pion is indicated by the logic coincidence signal $\bar{3} \cdot 4 \cdot \bar{5}$ during a 100 ns gate following the STOP signal which is defined to be an "EVENT". The anticoincidence signals on counters S_3 and S_5 eliminate other particles traversing the telescope after the STOP signal. The probability that a pion will be detected within this 100 ns gate is ϵ_π and will be discussed in section 3.2.

Fig.2.2 and Fig.2.3 are examples of histograms from a STOPS and an EVENTS run respectively. Fig.2.4 and Fig.2.5 are projections of these histograms onto the time of flight and energy loss axes for the same two runs.

Negative pions undergo atomic capture at a rate much higher than their decay rate, hence they could not be identified by the method described above and negative pion production cross sections could not be calculated.

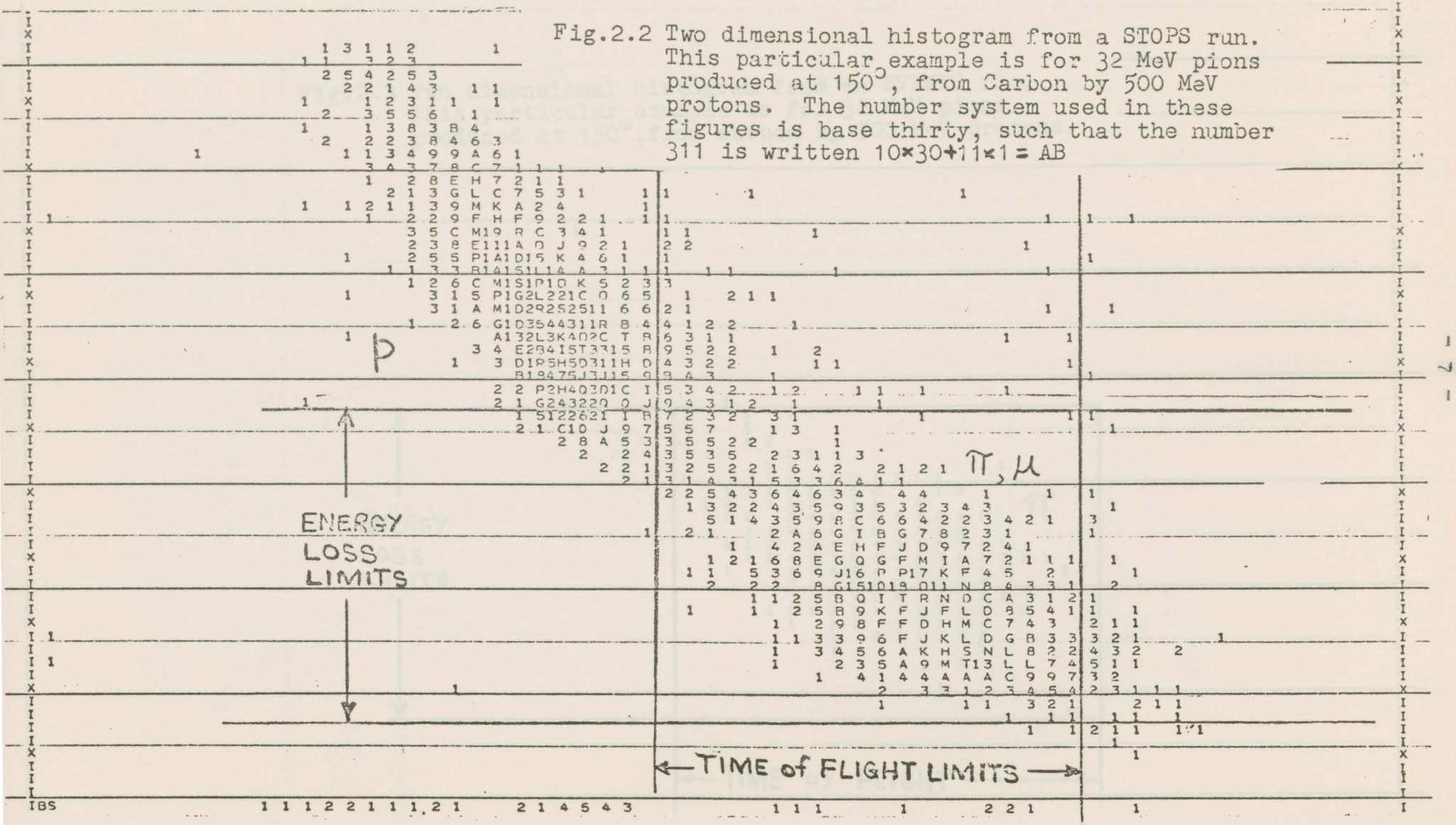

Fig.2.2 Two dimensional histogram from a STOPS run. This particular example is for 32 MeV pions produced at 150°, from Carbon by 500 MeV protons. The number system used in these figures is base thirty, such that the number 311 is written 10×30+11×1 = AB

Fig.2.3 Two dimensional histogram from an EVENTS run. This particular example is for 32 MeV pions produced at 150°, from carbon by 500 MeV protons.

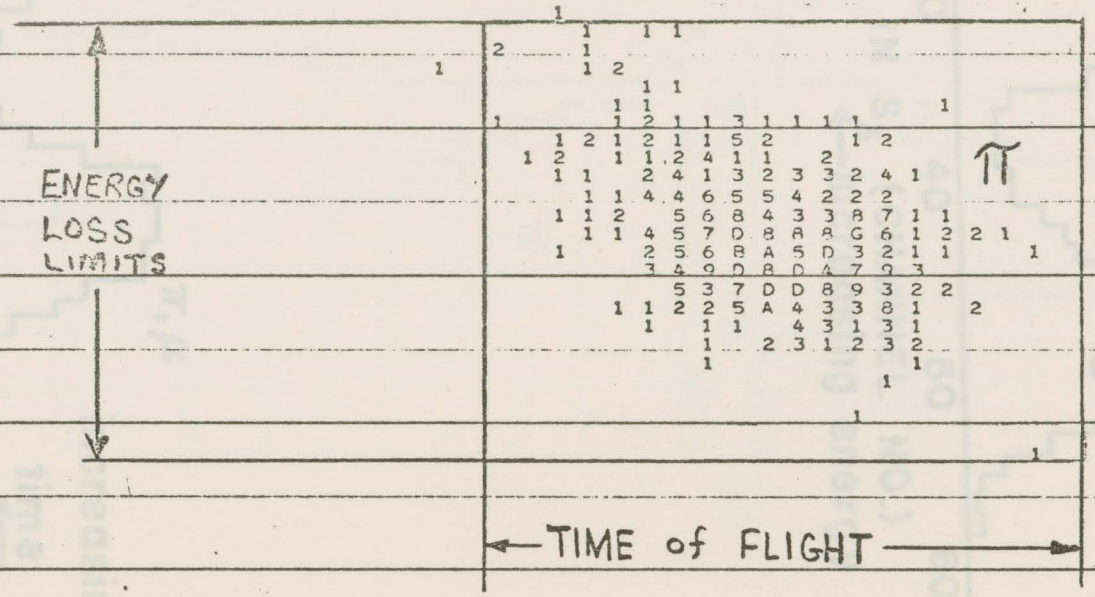

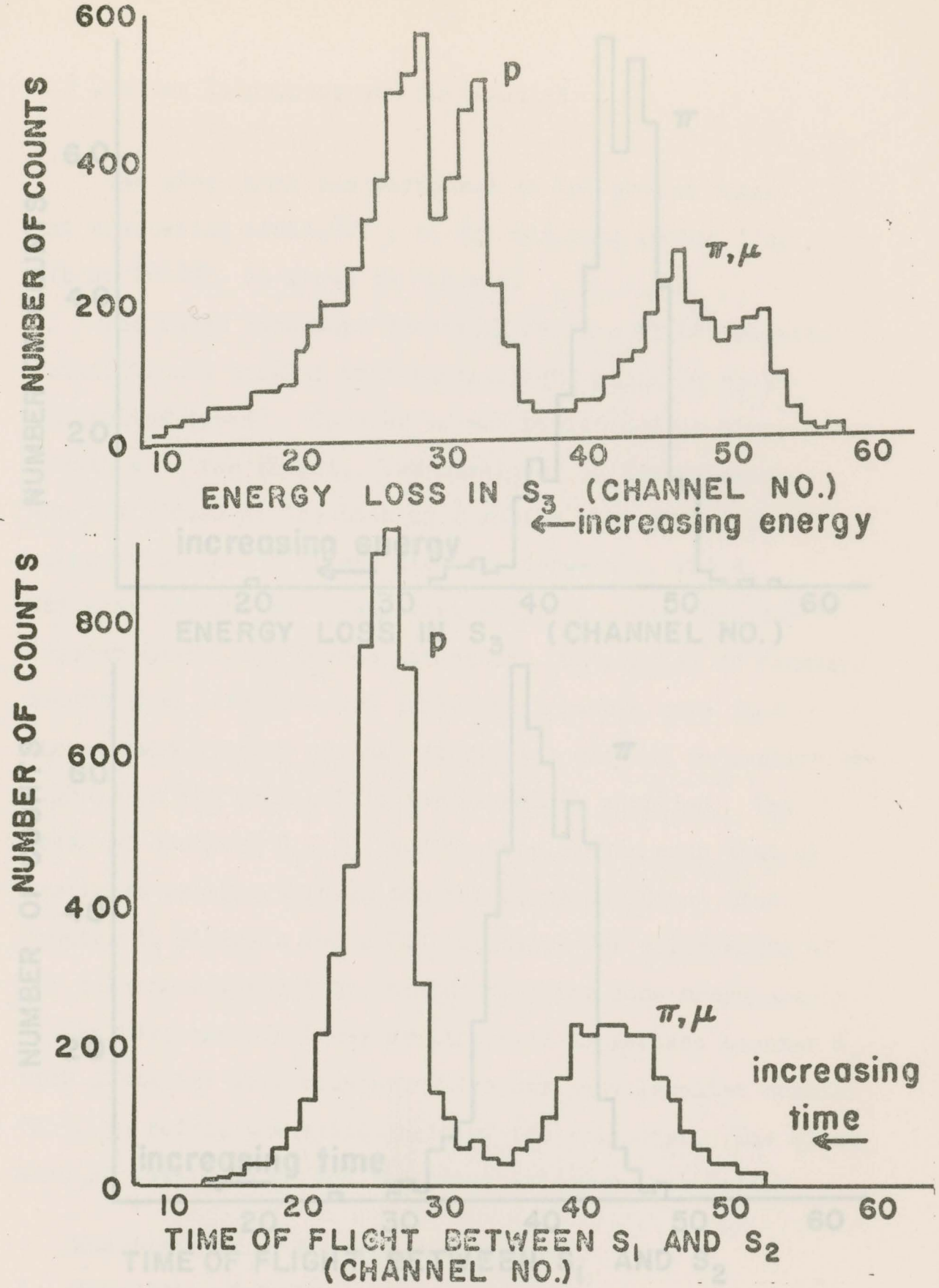

Fig.2.4 One dimensional histograms of energy loss in counter S_3 and Time of Flight between counters S_1 and S_2 for a STOPS run.

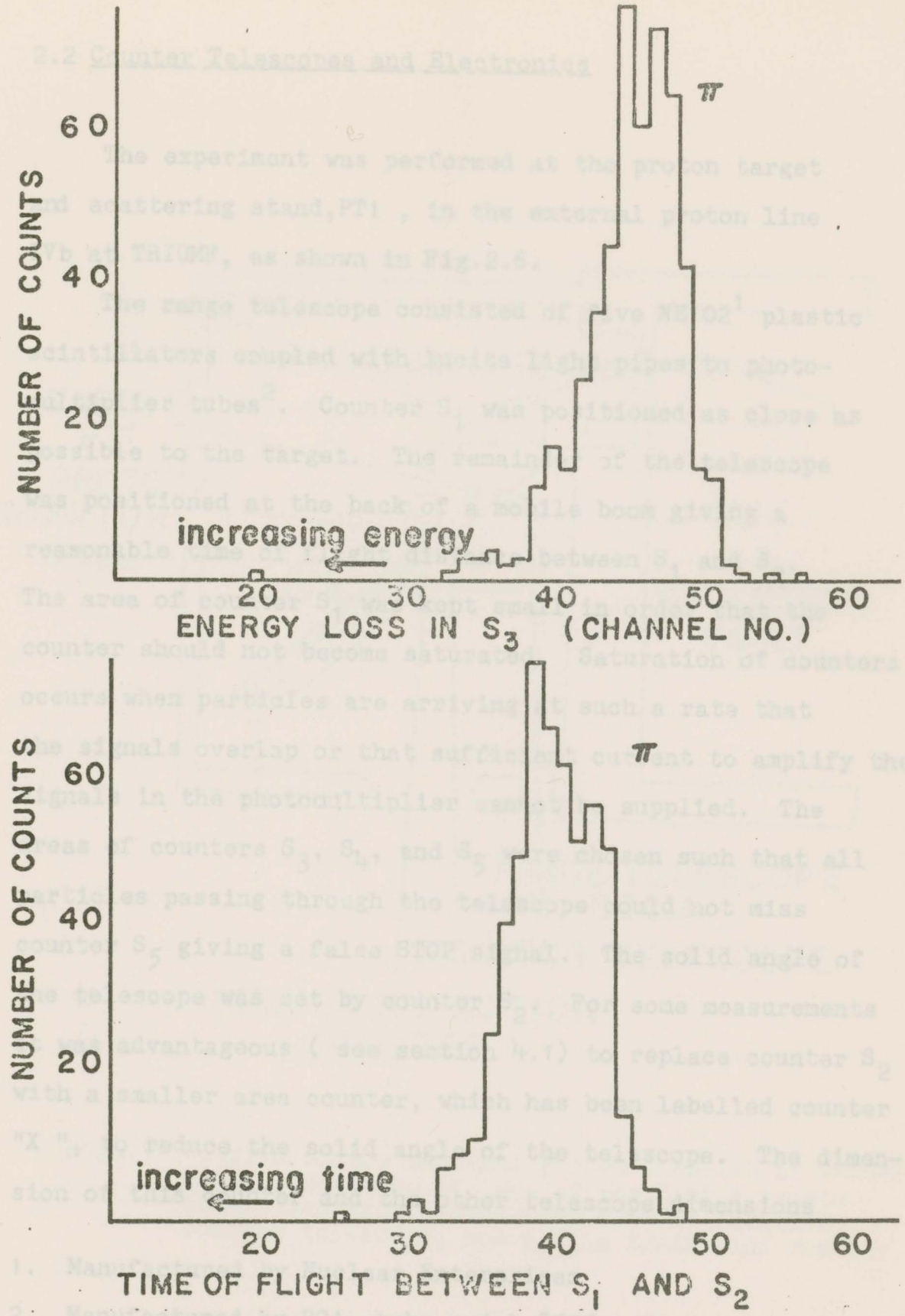

Fig.2.5 One dimensional histograms of energy loss in counter S_3 and Time of Flight between counters S_1 and S_2 for an EVENTS run.

2.2 Counter Telescopes and Electronics

The experiment was performed at the proton target and scattering stand, PT1 , in the external proton line IVb at TRIUMF, as shown in Fig.2.6.

The range telescope consisted of five NE102[1] plastic scintillators coupled with lucite light pipes to photomultiplier tubes[2]. Counter S_1 was positioned as close as possible to the target. The remainder of the telescope was positioned at the back of a mobile boom giving a reasonable time of flight distance between S_1 and S_2. The area of counter S_1 was kept small in order that the counter should not become saturated. Saturation of counters occurs when particles are arriving at such a rate that the signals overlap or that sufficient current to amplify the signals in the photomultiplier cannot be supplied. The areas of counters S_3, S_4, and S_5 were chosen such that all particles passing through the telescope could not miss counter S_5 giving a false STOP signal. The solid angle of the telescope was set by counter S_2. For some measurements it was advantageous (see section 4.1) to replace counter S_2 with a smaller area counter, which has been labelled counter "X ", to reduce the solid angle of the telescope. The dimension of this counter and the other telescope dimensions

1. Manufactured by Nuclear Enterprises
2. Manufactured by RCA, tube model 8575

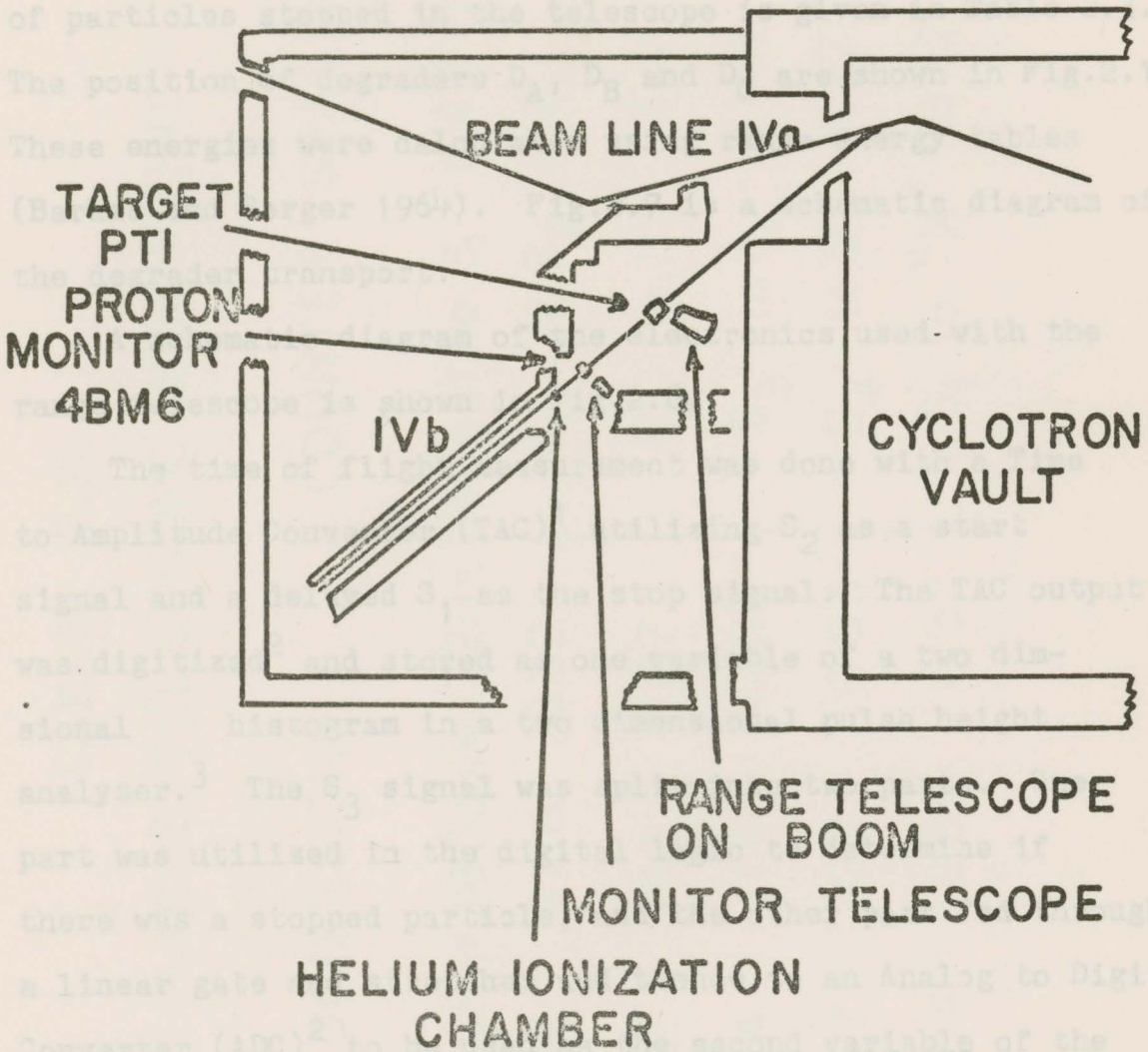

Fig.2.6 Diagram of the external proton line IVb at TRIUMF showing position of one of the U.of A.remote controlled boom, proton beam monitor location, monitor telescope, and helium ionization chamber.

are given in Table 2.2.

A remote control device was built to change the amount of copper degrader in the telescope. The dimensions of degraders available and the corresponding range in energy of particles stopped in the telescope is given in Table 2.3. The position of degraders D_A, D_B and D_C are shown in Fig.2.1. These energies were calculated using range energy tables (Barkas and Berger 1964). Fig.2.7 is a schematic diagram of the degrader transport.

A schematic diagram of the electronics used with the range telescope is shown in Fig.2.8.

The time of flight measurement was done with a Time to Amplitude Converter (TAC)[1], utilizing S_2 as a start signal and a delayed S_1 as the stop signal. The TAC output was digitized[2] and stored as one variable of a two dimsional histogram in a two dimensional pulse height analyzer.[3] The S_3 signal was split into two parts. One part was utilized in the digital logic to determine if there was a stopped particle, and the other part fed through a linear gate and stretcher and thence to an Analog to Digital Converter (ADC)[2] to be used as the second variable of the two dimensional histogram in the pulse height analyzer. An EVENT was recorded if a $\bar{3}\cdot4\cdot\bar{5}$ was observed during a 100 ns gate which was generated 22 ns after the end of the

1. Ortec model 437A TAC
2. Nuclear Data model GEN II ADC
3. Nuclear Data model 2400

TABLE 2.2

RANGE TELESCOPE DIMENSIONS

COUNTER DIMENSIONS

counter S_1	3.80cm	×3.80cm	×0.32cm
S_2	8.86	8.86	0.32
S_3	15.2	15.2	1.27
S_4	11.4	11.4	0.63
S_5	12.7	12.7	0.63
"X"	2.54	2.54	0.32

COUNTER SPACING

target to S_1	64.7cm
S_1 to S_2	186.1
S_2 to S_3	13.0
S_3 to S_4	4.43
S_4 to S_5	1.27
S_1 to "X"	167.2

TABLE 2.3

COPPER DEGRADER DIMENSIONS AND CORRESPONDING ENERGY BITES

DEGRADER D_A Cu (cm)	DEGRADER D_B Cu (cm)	DEGRADER D_C Cu (cm)	STOPPED π ENERGY -not including target- (MeV)	ENERGY BITE (MeV)	STOPPED π ENERGY -with 0.189 g/cm^2 C- (MeV)	ENERGY BITE (MeV)
no degraders			21.75	3.65	22.69	3.54
		0.32	31.26	2.97	32.00	2.93
0.95		0.32	52.81	2.24	53.35	2.22
2.22		0.32	75.68	1.88	76.13	1.88
2.22	1.59	0.32	101.24	1.72	101.65	1.72

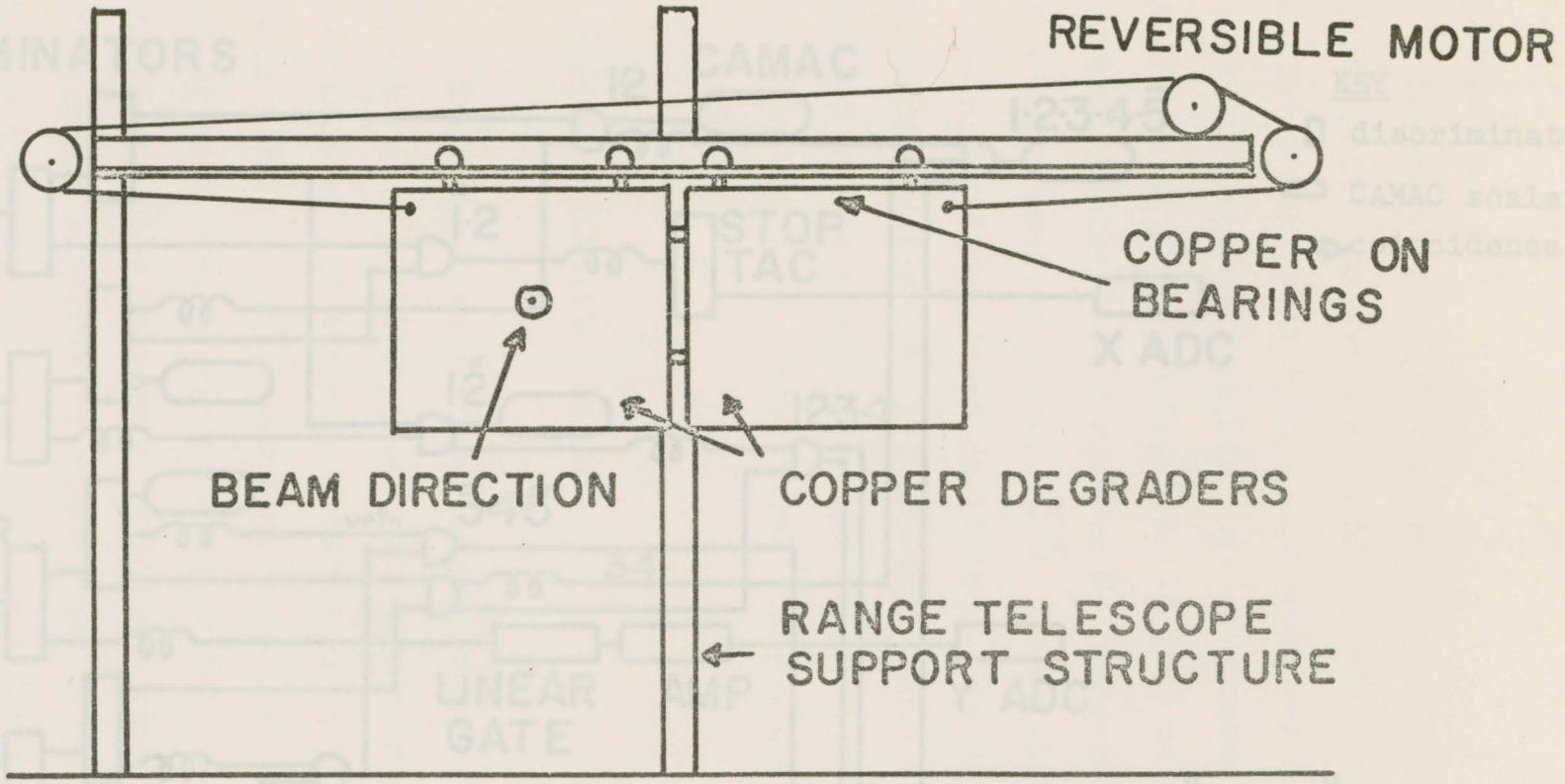

Fig. 2.7 Schematic diagram of the copper degrader transport. Each pair of degraders are mounted on bearings and are moved under the control of a reversible 110 volt motor. Positions of the degraders are indicated by a series of microswitches.

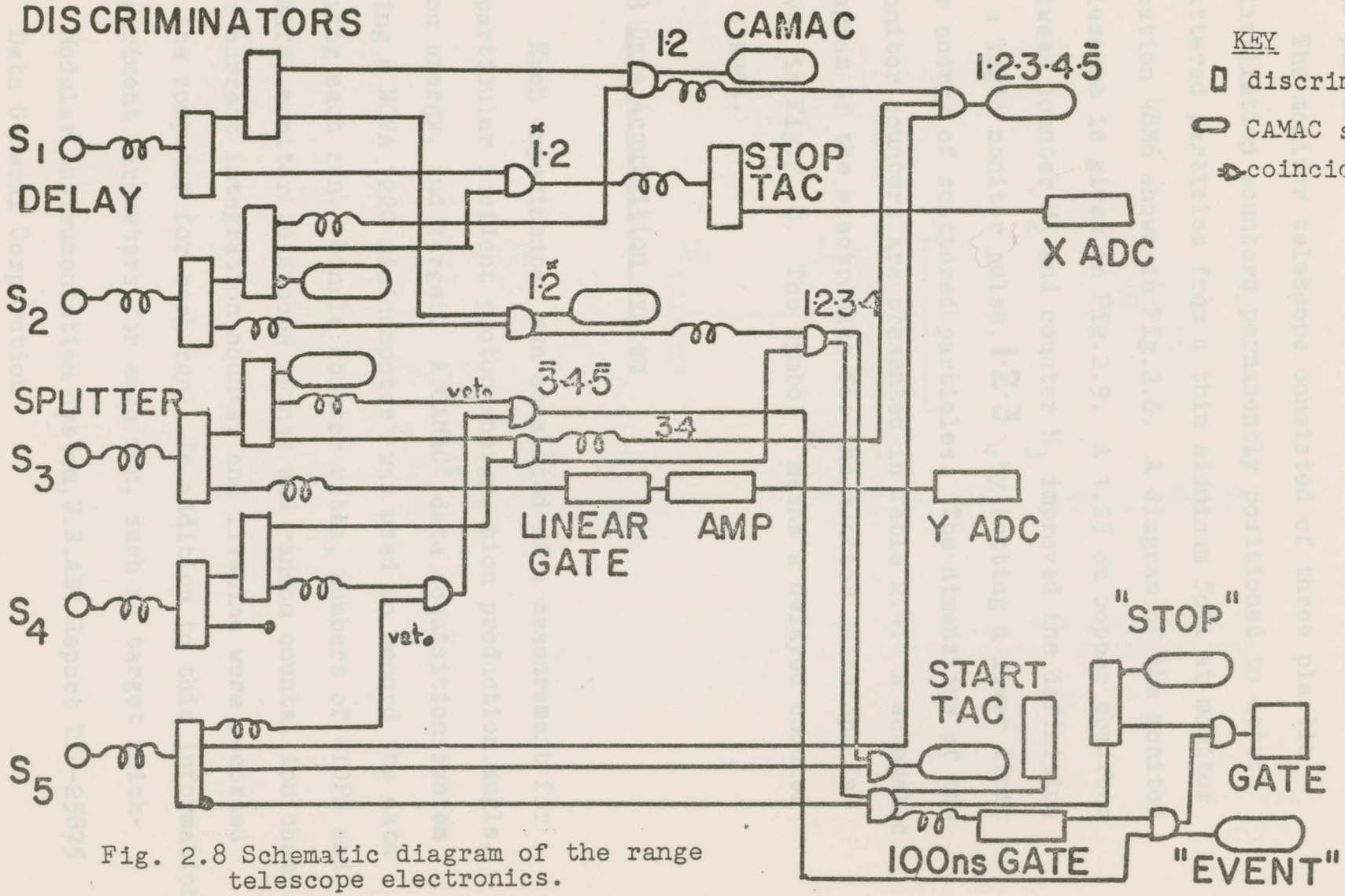

Fig. 2.8 Schematic diagram of the range telescope electronics.

STOP pulse.

The monitor telescope consisted of three plastic scintillation counters permanently positioned to detect scattered particles from a thin aluminum foil at monitor location 4BM6 shown in Fig.2.6. A diagram of the monitor telescope is given in Fig.2.9. A 1.25 cm copper absorber between counter M_2 and counter M_3 improved the definition of a logic monitor pulse, $1 \cdot 2 \cdot 3$, by setting a lower limit for energy of scattered particles. The dimensions of the monitor counters are presented in Table 2.4. A schematic diagram of the electronics for the monitor telescope is given in Fig.2.10. The symbol $\tilde{1}$ means a delayed counter M_1 signal.

2.3 Data Acquisition System

Each experimental run consisted of a measurement for a particular incident proton energy, pion production angle, pion energy, and target. A CAMAC[1] data acquisition system using a NOVA 1220 minicomputer[2] was used to record the data during each run. Single counter rates, numbers of STOPS and EVENTS, monitor telescope counts and random counts, ion chamber current integration counts, and livetime were recorded in the computer for each run. In addition to this information experiment parameters for each run, such as target thick-

1. Modular Instrumentation System, U.S.AEC Report TID-25875
2. Data General Corporation

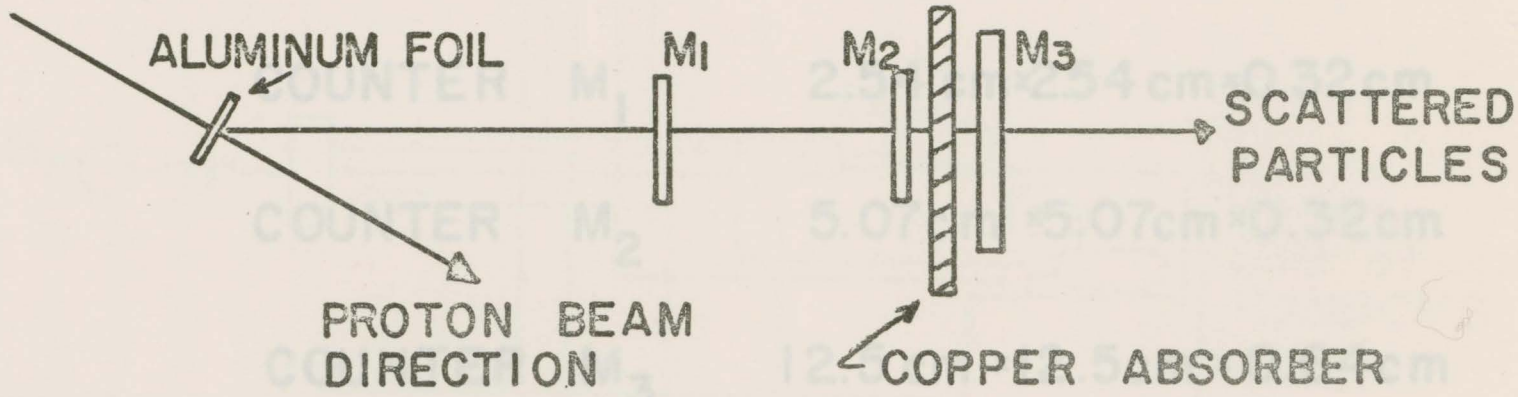

Fig. 2.9 Schematic diagram of the three element monitor telescope showing scattering foil, counters and copper degrader.

TABLE 2.4

DIMENSIONS OF THE MONITOR COUNTERS

COUNTER	M_1	2.54 cm×2.54 cm×0.32 cm
COUNTER	M_2	5.07 cm ×5.07 cm×0.32 cm
COUNTER	M_3	12.5 cm ×12.5 cm × 0.64 cm

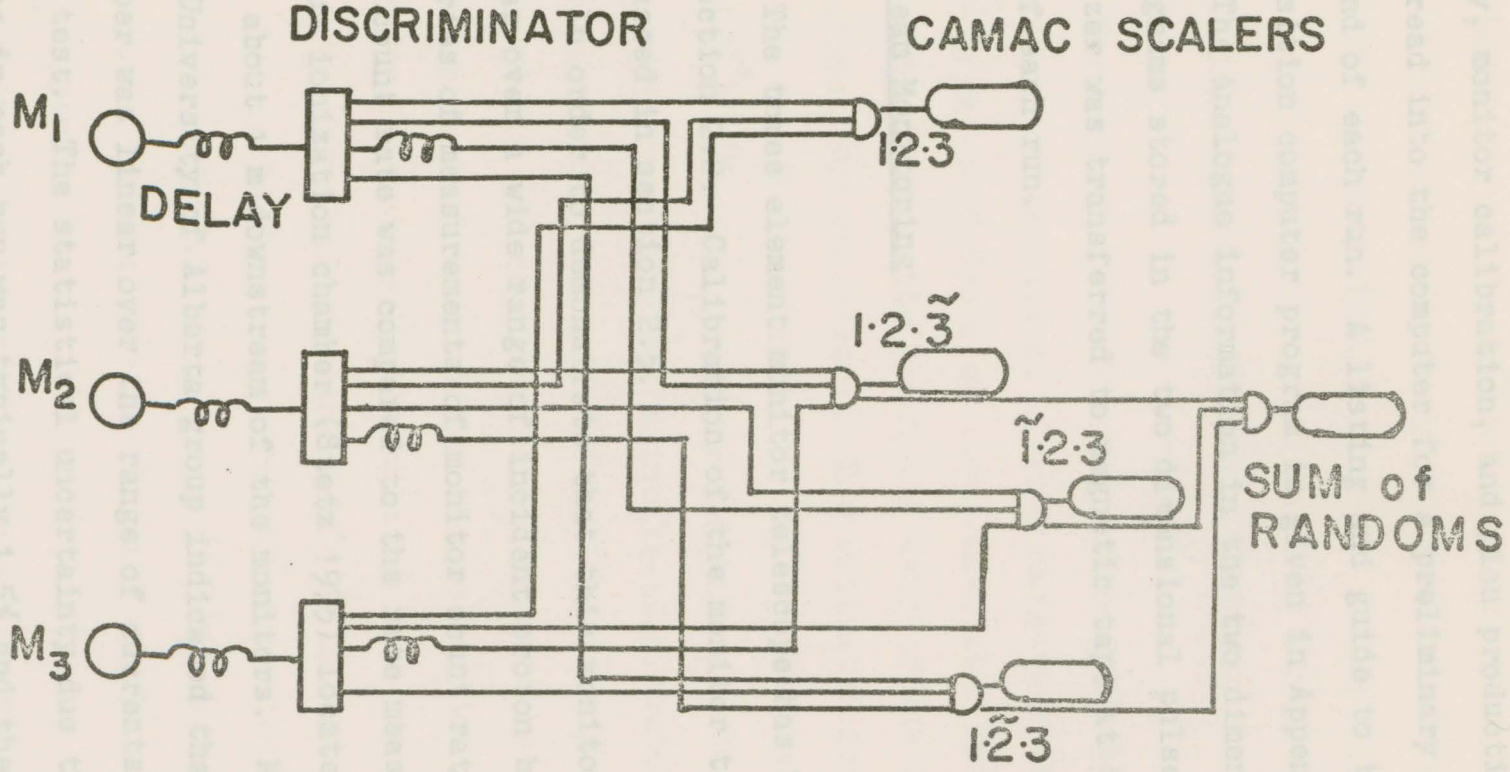

Fig.2.10 Schematic diagram of the monitor telescope electronics.

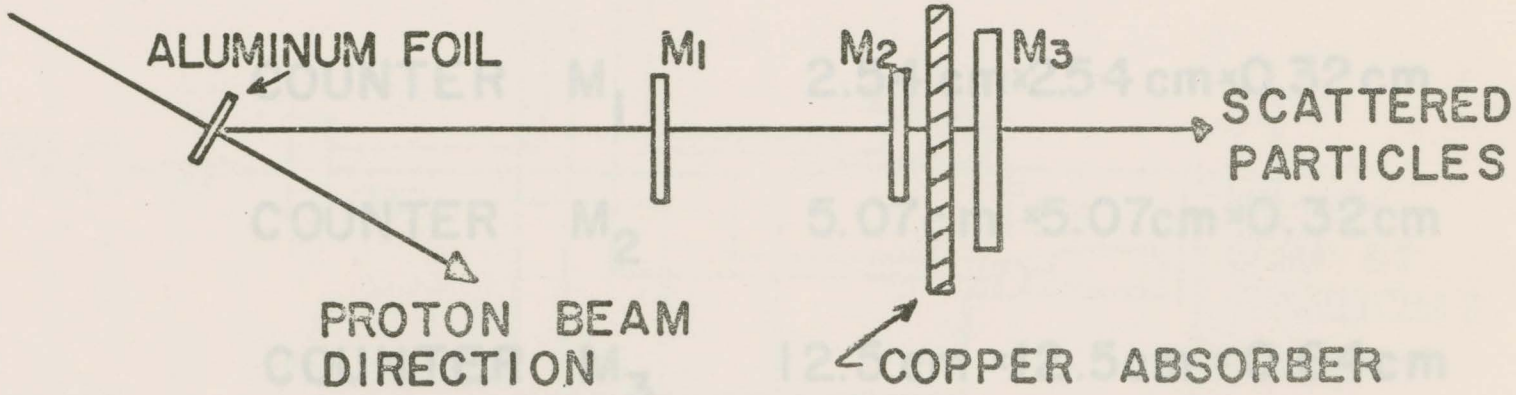

Fig. 2.9 Schematic diagram of the three element monitor telescope showing scattering foil, counters and copper degrader.

ness, and material, stopped pion energy, incident proton energy, monitor calibration, and pion production angle, were read into the computer for a preliminary analysis at the end of each run. A listing and guide to the data acquisition computer program is given in Appendix A.

The analogue information in the two dimensional histograms stored in the two dimensional pulse height analyzer was transferred to magnetic tape at the completion of each run.

2.4 Beam Monitoring

The three element monitor telescope has been described in section 2.2. Calibration of the monitor telescope is discussed in section 2.5.

In order to demonstrate that this monitoring scheme was linear over a wide range of incident proton beam intensities, a series of measurements of monitor count rate was made. This count rate was compared to the rate measured with a helium ionization chamber (Stetz 1975) located in the proton beam about 1 m downstream of the monitors. Measurements by the University of Alberta group indicated that the ion chamber was linear over the range of currents used during this test. The statistical uncertainty due the numbers of counts in each run was typically 1.5% and the standard deviation in random corrected monitor counts was only 0.6%. Ion chamber counts were recorded throughout the experiment and provided a check on all monitor calibrations.

During a 100 μs period following a STOP pulse the discriminators of the monitor counters were shut off so that no monitor counts would be recorded while the range telescope was inactive.

2.5 Calibration of the Monitor Telescope

The monitor telescope was calibrated absolutely by an activation technique. Carbon targets with areal density 0.344 g/cm^2 or 0.858 g/cm^2 were activated for a short time with a beam intensity about the same range as that used throughout the experiment. The activated foils were placed between two aluminum foils so that positrons from the decay $^{11}C(\beta^+)^{11}B$ would promptly annihilate. The foils were placed adjacent to a NaI scintillation counter which was used to observe the 0.51 MeV annihilation gamma rays. Repeated 200 second pulse height spectra were recorded on tape for several hours after the activation. The number of incident protons was calculated from the known $^{12}C(p,pn)^{11}C$ cross sections and the number of ^{11}C nuclei produced which was calculated from the number of annihilation gamma rays observed. Fig.2.11 is a graph of ^{11}C production cross sections (Cumming 1963). Details of the calculation are given Appendix B.

In order to check the method of recording pulse height spectra and background subtraction in the ASPEC computer

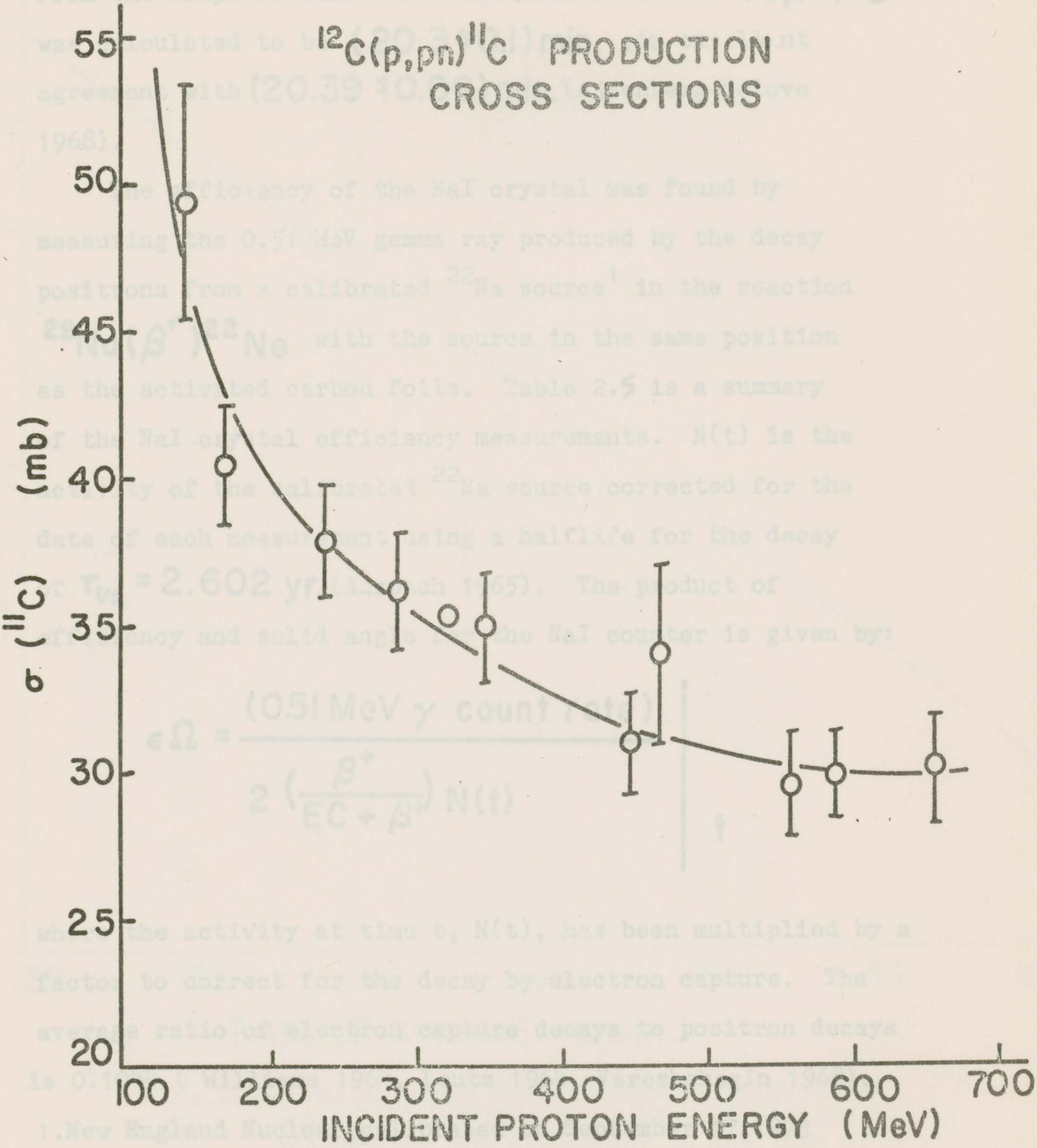

Fig.2.11 Graph of ^{11}C production cross sections based on a review by Cummings (1963)

code, the areas of the 0.51 MeV gamma peaks for a series of spectra have been plotted against time in Fig.2.12. From the slope of this curve the half life for $^{11}C(\beta^+)^{11}B$ was calculated to be (20.3 ± 0.1) min. , in excellent agreement with (20.39 ± 0.06) min. (Ajzenberg-Selove 1968).

The efficiency of the NaI crystal was found by measuring the 0.51 MeV gamma ray produced by the decay positrons from a calibrated ^{22}Na source[1] in the reaction $^{22}Na(\beta^+)^{22}Ne$ with the source in the same position as the activated carbon foils. Table 2.5 is a summary of the NaI crystal efficiency measurements. N(t) is the activity of the calibrated ^{22}Na source corrected for the date of each measurement using a halflife for the decay of $\tau_{1/2} = 2.602$ yr. (Anspach 1965). The product of efficiency and solid angle for the NaI counter is given by:

$$\epsilon\Omega = \left. \frac{(0.51\,\text{MeV}\ \gamma\ \text{count rate})}{2\left(\frac{\beta^+}{EC+\beta^+}\right) N(t)} \right|_t$$

where the activity at time t, N(t), has been multiplied by a factor to correct for the decay by electron capture. The average ratio of electron capture decays to positron decays is 0.1044 (Williams 1964, Leutz 1964, Vereshchagin 1968).

1. New England Nuclear, calibrated on September 17, 1973

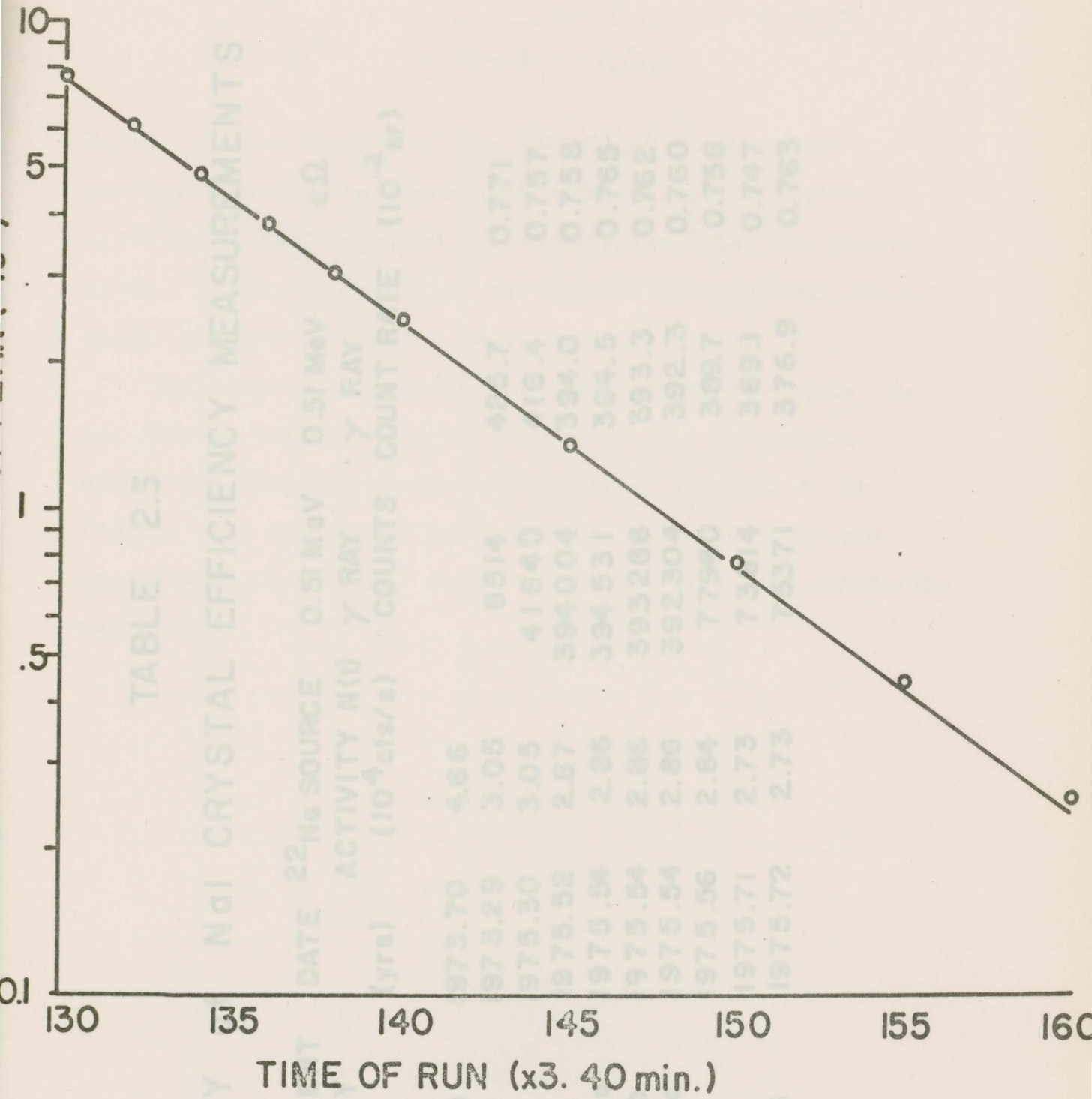

Fig.2.12 Semilog graph of the area of the 0.51 MeV annihilation gamma ray peak, with background subtraction, as a function of the time of each observation.

TABLE 2.5

SUMMARY of NaI CRYSTAL EFFICIENCY MEASUREMENTS

MEASUREMENT IDENTITY	DATE (yrs)	^{22}Na SOURCE ACTIVITY N(t) (10^4cts/s)	0.51 MeV γ RAY COUNTS	0.51 MeV γ RAY COUNT RATE	$\epsilon\Omega$ (10^{-2}sr)
calibration	1973.70	4.66			
TRX2	1975.29	3.05	8514	425.7	0.771
TRX5	1975.30	3.05	41640	416.4	0.757
TRX9	1975.52	2.87	394004	394.0	0.758
TRX10a	1975.54	2.86	394531	394.5	0.765
TRX10b	1975.54	2.86	393286	393.3	0.762
TRX10c	1975.54	2.86	392304	392.3	0.760
TRX11	1975.56	2.84	77940	389.7	0.758
TRX14	1975.71	2.73	73814	369.1	0.747
TRX16	1975.72	2.73	75371	376.9	0.763

The ratio of beta decays to total decays is:

$$\frac{\beta^+}{EC + \beta^+} = \frac{1.000}{0.1044 + 1.000} = 0.905$$

Table 2.6 is a summary of the activation measurements performed during the experiment. The monitor counters after April used improved photomultiplier tubes for higher rates. Other variations in the monitor calibrations reflect small changes in monitor geometry between runs.

For those runs when the ion chamber was available, an ion chamber current gain was calculated for comparison with p-p scattering measurements made by Kitching et al (1975). The calculated gains were in good agreement and provided an independent check on the absolute beam monitoring calibration.

TABLE 2.6

SUMMARY OF ACTIVATIONS FOR MONITOR CALIBRATIONS

ACTIVATION IDENTIFICATION	PROTON ENERGY (MeV)	PROTON CURRENT (10^{10} p/s)	MONITOR RATE (cts/s)	PROTONS PER MONITOR COUNT
TRLY (22/3/75)	500	3.94	$4.63 \cdot 10^{4}$	$8.51 \cdot 10^{5}$
TRX6 (24/4/75)	500	2.98	$3.31 \cdot 10^{4}$	$9.00 \cdot 10^{5}$
TRX7 (4/7/75)	500	4.12	$6.12 \cdot 10^{3}$	$6.73 \cdot 10^{6}$
TRX 9 (11/7/75)	500	2.56	$3.90 \cdot 10^{3}$	$6.56 \cdot 10^{6}$
TRX11 (26/7/75)	500	2.76	$3.98 \cdot 10^{3}$	$6.94 \cdot 10^{6}$
TRX2 (15/4/75)	450	1.45	$1.55 \cdot 10^{4}$	$9.55 \cdot 10^{5}$
TRX18 (2/10/75)	450	2.49	$3.26 \cdot 10^{3}$	$7.63 \cdot 10^{6}$
TRX16 (18/9/75)	400	1.42	$1.40 \cdot 10^{3}$	$10.2 \cdot 10^{6}$

CHAPTER 3

CALCULATION OF CROSS SECTIONS

3.1 Differential Cross Sections

The cross sections were calculated using the equation:

$$\frac{d^2\sigma}{dT_\pi d\Omega} = \frac{N_\pi f_\pi}{(N_t/\cos\alpha) N_p \Omega \Delta T_\pi \epsilon_\pi \epsilon_d \epsilon_a \epsilon_{el} \epsilon_m} \qquad (3.1)$$

where N_π is the number of events detected by the range telescope. These are simply the stopped particles with a pion decay detected. f_π is the correction for proton contamination as found from the two dimensional histograms. This correction eliminates false EVENT signals generated by a stopped proton and a pion which had previously stopped but took longer than 100 ns to decay. N_t is the number of target atoms per unit area. Table 3.1 contains a list of N_t for the targets used in the experiment. α is the target angle as shown in Fig.3.1. N_p is the number of protons incident on the target as determined by the product of the number of monitor counts for that run and the monitor calibration for that series of runs. Ω is the geometrical solid angle of the pion range telescope. The solid angle was determined by the counter in the S_2 position. The normal telescope had a solid angle of (1.25 ± 0.01) msr. and the telescope with the "X" counter had a solid angle of $(1.19 \pm 0.01) \cdot 10^{-1}$ msr.

TABLE 3.1

TARGET PARAMETERS

IDENTIFICATION OF TARGET (mnemonic)	AREAL DENSITY (g/cm^2)	N_t (atoms/μb)
U.of A. Carbon (UACA)	0.20	$1.01 \cdot 10^{-8}$
UVIC Carbon (UVCA)	0.378	$1.91 \cdot 10^{-8}$
UVIC Cu "A" (VCUA)	0.591	$5.61 \cdot 10^{-9}$
UVIC Cu "THIN" (THCU)	0.149	$1.43 \cdot 10^{-9}$
U.of A. CH_2 (UACH)	0.189	$8.14 \cdot 10^{-9}$
UVIC CH_2 (UVCH)	0.147	$6.32 \cdot 10^{-9}$

all target areas = $5 \times 5 cm^2$

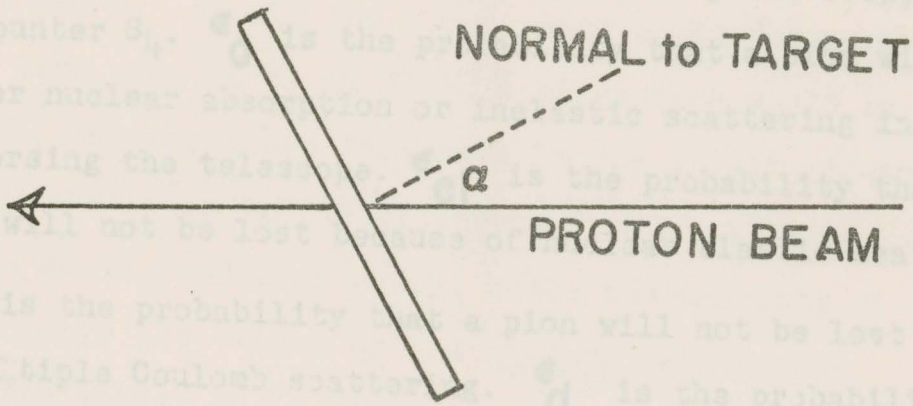

Fig. 3.1 Orientation of target showing definition of target angle.

as given by the Monte Carlo program REVMOC (Kitching 1971) which included the effect of pions originating throughout the target. ΔT_π is the energy acceptance of the pion range telescope as discussed in section 2.2. ϵ_π is the pion detection efficiency which is simply the ratio of pions detected to the number of pions stopped in counter S_4. ϵ_a is the probability that a pion will not suffer nuclear absorption or inelastic scattering in traversing the telescope. ϵ_{el} is the probability that a pion will not be lost because of nuclear elastic scattering. ϵ_m is the probability that a pion will not be lost because of multiple Coulomb scattering. ϵ_d is the probability that a pion will not decay in the telescope before it stops in counter S_4. The estimation of the efficiency factors ϵ_π through ϵ_m are discussed in the following sections.

3.2 Pion Detection Efficiency

The probability that a pion will decay during a (100 ± 1) ns period beginning (22.0 ± 0.5) ns after stopping in counter S_4 is given by:

$$\epsilon_\pi = \int_{22.0\pm.5}^{122\pm1} \frac{\exp(-t/\tau_\pi)}{\tau_\pi}\, dt = (0.41 \pm 0.01)$$

The pion lifetime is $\tau_\pi = 26.03 \pm 0.02$ ns (Chaloupka 1974). The probability that muon will decay in the same

gate is given by:

$$\epsilon_\mu = \int_{22.0 \pm .5}^{122 \pm 1} \frac{\exp(-t/\tau_\mu)}{\tau_\mu}\, dt = 0.04$$

The muon lifetime is $\tau_\mu = 2199.4$ ns (Particle Data Group 1974). If all the muons which could decay within the gate were counted as an EVENT a correction would be required, however there is a much larger amount of kinetic energy available to the electrons from muon decay than to the muons from pion decay, hence the majority of the muon decays are vetoed by the $\bar{3}.4.\bar{5}$ requirement.

The values of ϵ_π used was based on actual measurements at SREL and Berkeley (James 1974), which indicated $\epsilon_\pi = 0.39 \pm 0.01$ in agreement with the above calculated probability.

3.3 Pion Decay Correction

A correction for the number of pions which decay in the telescope before being detected as pion events has been included in the cross sections. This correction was calculated from:

$$\epsilon_d = \int_T^\infty \frac{\exp(-t/\tau_\pi)\, dt}{\tau_\pi} = \exp(-T/\tau_\pi)$$

Where T is given by:

$$T = \Sigma t_i + \Sigma t_s$$

The t_i are the flight times in the i^{th} air drift of the telescope and are given by:

$$t_i = \frac{l_i (1-\beta_i^2)^{1/2}}{\beta_i c}$$

where l_i is the length of the i^{th} drift and β_i is the mean velocity in that drift divided by the speed of light, c.

The second term in the expression for T is the stopping time in the telescope and t_s is given by:

$$t_s = \frac{M_o c^2}{c} \int_{\beta_{s1}}^{\beta_{s2}} \frac{d\beta}{\rho(1-\beta^2)\, dT_\pi/dx}$$

where M_o is the pion rest mass, $\beta_{s1}c$ and $\beta_{s2}c$ are the initial and final mean velocities in telescope element s; ρ is the density of telescope element s; and dT/dx is the rate of energy loss per unit areal density for pions in telescope element s. The t_s for each telescope element was calculated by a Simpson's rule integration with the range in β separated into twenty parts.

The values of the pion decay correction ϵ_d are summarized in Table 3.2.

3.4 Corrections for Nuclear Effects in the Telescope

The probability that pions were not detected due to nuclear inelastic scattering or absorption, and nuclear elastic scattering are discussed in sections 3.4.1 and 3.4.2. The fraction of stopping pions which initially had too high an energy to stop in counter S_4 but which interacted inelastically in the material in front of counter S_4 resulting in a false EVENT was considered to be insignificant for this geometry of telescope (James 1975).

3.4.1 Nuclear Absorption and Inelastic Scattering Corrections

ϵ_a is the probability that a pion was not detected due to the effects of nuclear absorption or nuclear inelastic scattering. This probability is given by:

$$\epsilon_a = \exp\left(\frac{-N_o}{A}\int_0^{T_\pi}\frac{\sigma_a\,dT}{dT/dx}\right)$$

where No is Avogadro's Number, A is the atomic weight of the material, σ_a is the total reaction cross section for nuclear absorption and inelastic scattering, and dT/dx is the rate of energy loss per unit areal density for pions. The integration was performed numerically using Simpson's method with the integral broken into twenty parts. The values of σ_a and dT/dx were stored in the integration program as a function of T and the material. The total reaction

cross sections were taken from a compilation of available data in the pion energy range less than 300 MeV (James 1975). The computed values of ϵ_a for each stopped pion energy are given in Table 3.2.

3.4.2 Nuclear Elastic Scattering Corrections

ϵ_{el} is the probability that a pion was not detected due to the effect of nuclear elastic scattering. This probability is given by:

$$\epsilon_{el} = 1 - \alpha(1-\epsilon_s)$$

where α is the fraction of elastically scattered particles which miss counter S_4 and ϵ_s is the probability that a pion was not elastically scattered. ϵ_s was calculated by the same method as ϵ_a using the equation:

$$\epsilon_s = \exp\left(\frac{-N_o}{A} \int_0^{T_\pi} \frac{\delta \sigma_a \, dT}{dT/dx} \right)$$

where δ is the observed ratio of the total nuclear elastic scattering cross section, σ_{el} to σ_a . δ was taken to be 0.6 ± 0.1 (Kessler and Lederman 1954, Dzhelepov et al 1957, Koltun 1969, and Binon et al 1970). For this telescope geometry α has been estimated to be 0.2 ± 0.1 (James 1975). The computed values of ϵ_s and ϵ_{el} are given in Table 3.2

3.5 Coulomb Multiple Scattering

As a charged particle travels through the range telescope it is repeatedly scattered by the Coulomb field of each nucleus it passes. In this manner particles which enter a single foil as a narrow, parallel beam emerge with an angular distribution and larger displacements from the central trajectory. The computer code, REVMOC (Kitching 1971) is a Monte Carlo program which will track particles through a system of counters and absorbers first considering geometrical effects and separately adding the effect of Coulomb scattering using distributions in angle and displacements calculated by Molière (1959).

The probability ϵ_m that a pion is not lost due to Coulomb multiple scattering is

$$\epsilon_m = N_f / N_i$$

where N_i is the number of particles travelling through the telescope within its geometrical limits, and N_f is the number of particles which went through the end of the telescope counter S_4, when multiple scattering was calculated. The values of ϵ_m are given in Table 3.2.

3.6 Discussion of Uncertainties

In the cross section calculation, the uncertainties of some of the variables discussed in this chapter are relative, varying from run to run or between different pion

TABLE 3.2

VALUES OF CORRECTION FACTORS

STOPPED π ENERGY (MeV)	π DECAY CORRECTION ϵ_d	NUCLEAR ABSORPTION ϵ_a	NUCLEAR ELASTIC SCATTERING ϵ_s	ϵ_{el}	COULOMB SCATTERING ϵ_m
22.69	0.533 ±0.005	0.993 ±0.001	0.996 ±0.001	0.999 ±0.001	0.701 ±0.012
32.00	0.606 ±0.006	0.980 ±0.002	0.988 ±0.002	0.998 ±0.001	0.833 ±0.015
53.34	0.685 ±0.007	0.928 ±0.007	0.956 ±0.007	0.991 ±0.004	0.725 ±0.017
76.13	0.734 ±0.007	0.844 ±0.014	0.903 ±0.015	0.981 ±0.010	0.700 ±0.014
101.65	0.772 ±0.008	0.735 ±0.021	0.831 ±0.025	0.966 ±0.017	0.747 ±0.014

energies. Other uncertainties are absolute and are common to all the measurements.

The major relative uncertainties arise from counting statistics in N_π and f_π which vary between 2 and 5%. At some forward angle measurements the values of f_π were taken from higher statistics runs with the same production angle and pion eneegy. The uncertainty in target angle was $\pm 0.1^\circ$ and was considered insignificant. The absorber and counter thicknesses and dimensions were well known hence uncertainties in ΔT_π were considered about 1%, due mainly the uncertainties of the range energy loss tables and the lower level bias on the discriminator for counter S_4. The uncertainties in ϵ_d were estimated to be about 1%, also due the uncertainties in the range energy loss calculations, which set the integration limits. The uncertainties in ϵ_a and ϵ_{el} vary between 1 and 2% for increasing pion energy and are due the estimated 10% uncertainty in σ_a. The uncertainties quoted in ϵ_m are statistical only arising from the number of rays in the Monte Carlo program which were accepted into counter S_4.

The largest absolute uncertainty arises from the monitor calibration. This 7% uncertainty is dominated by the estimated 5% uncertainty in the ^{11}C production total cross sections. The measuring uncertainties in N_t were approximately 0.1% and hence were neglected. The 3% uncertainty in ϵ_π is a result of the measurements of pion detection efficiency. The uncertainty in solid angle Ω is less than

0.5%. The effect of the slightly distributed source was checked by comparing the solid angle from the REVMOC calculation with the geometrical calculation. No significant differences were observed.

3.7 Sample Calculation

The differential cross section for 32.0 MeV positive pions produced at an angle of 150°, from carbon is calculated in this section. The incident proton energy for this case was 500 MeV. The histogram for an adjacent STOPS run, shown in Fig.2.2, gave time of flight and energy loss limits for use in the EVENTS run, histogram shown in Fig.2.3, to find $f_\pi = 0.99 \pm 0.02$. From the monitor calibration for that series of runs and the number of monitor counts for that run, N_p was found to be:

$$N_p = (9.0 \pm 0.6) \cdot 10^5 \ \frac{\text{protons}}{\text{monitor counts}} \ (9.807 \cdot 10^6) \text{monitor counts}$$

$$= (8.8 \cdot 10^{12}) \text{protons}$$

The other parameters for this run are listed below.

$N_\pi = 538 \pm 23$ $\qquad \epsilon_\pi = 0.39 \pm 0.01$

$N_t = (1.01 \pm 0.01) \cdot 10^{-8}$ atoms/μb

$\alpha = (20.0 \pm 0.1)°$ $\qquad \epsilon_d = 0.606 \pm 0.006$

$\Omega = (1.25 \pm 0.01) \cdot 10^{-3}$ sr

$\Delta T_\pi = (2.93 \pm 0.03)$ MeV

$\epsilon_a = (0.98 \pm 0.01)$ $\qquad \epsilon_{el} = 1.00 \pm 0.01$

$\epsilon_m = (0.83 \pm 0.02)$

Using equation 3.1, the differential cross section for this case is:

$$\frac{d^2\sigma}{dT_\pi d\Omega} = (7.99 \pm 0.76)\,\mu b/MeV\cdot sr$$

The uncertainty quoted includes all absolute and relative uncertainties discussed in section 3.6.

CHAPTER 4

ANALYSIS OF TWO BODY MEASUREMENTS

The monitor calibration, energy bites, and pion detection efficiency of the telescope were checked by a measurement of $d\sigma/d\Omega$ for the reaction $p(p,\pi)D$, for several pion energies for which the cross section has been independently estimated using energy dependent fits to the total cross section. At each of the incident proton energies 400,450 and 500 MeV, production angles were selected which produced pions of energy lying within the energy bites of the telescope. The kinematics of this calculation are considered in section 4.1.1. Not all of the stopped pion energies could be measured at each of the incident proton energies because of the physical limitations of the scattering chamber. To ensure that the maximum pion yield was being detected for a particular pion telescope energy, an angular distribution was measured about the calculated production angle. This method was used rather than varying the primary proton energy in small steps because changing the angle was faster than incrementing the proton energy. An angular distribution for the case of pions produced by 450 MeV protons in the vicinity of 82° has been plotted in Fig.4.1. This figure clearly shows a background contribution from the carbon which is present in the CH_2 target as well as at lower angles from the reaction $p(p,p\pi)n$.

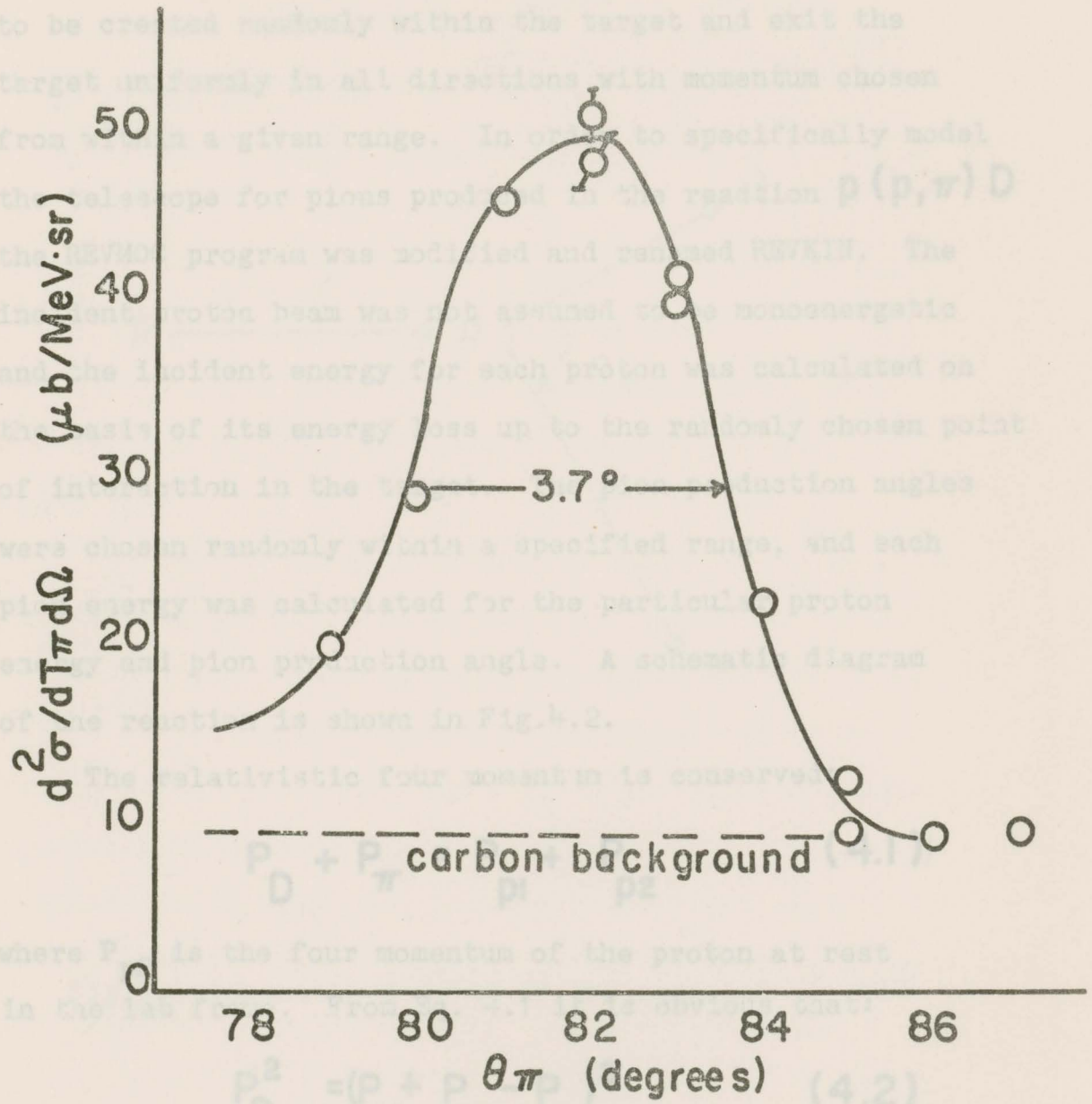

Fig.4.1 Observed angular distribution of pions produced by bombarding a CH_2 target with 450 MeV protons.

4.1 Calculation of Differential Cross Sections

4.1.1 Two Body Kinematics and Related Factors.

The Monte Carlo program REVMOC normally would be used to model the range telescope. In REVMOC pions are assumed to be created randomly within the target and exit the target uniformly in all directions with momentum chosen from within a given range. In order to specifically model the telescope for pions produced in the reaction $p(p,\pi)D$ the REVMOC program was modified and renamed REVKIN. The incident proton beam was not assumed to be monoenergetic and the incident energy for each proton was calculated on the basis of its energy loss up to the randomly chosen point of interaction in the target. The pion production angles were chosen randomly within a specified range, and each pion energy was calculated for the particular proton energy and pion production angle. A schematic diagram of the reaction is shown in Fig.4.2.

The relativistic four momentum is conserved:

$$P_D + P_\pi = P_{p1} + P_{p2} \qquad (4.1)$$

where P_{p2} is the four momentum of the proton at rest in the lab frame. From Eq. 4.1 it is obvious that:

$$P_D^2 = (P_{p1} + P_{p2} - P_\pi)^2 \qquad (4.2)$$

and hence a relation between the pion production

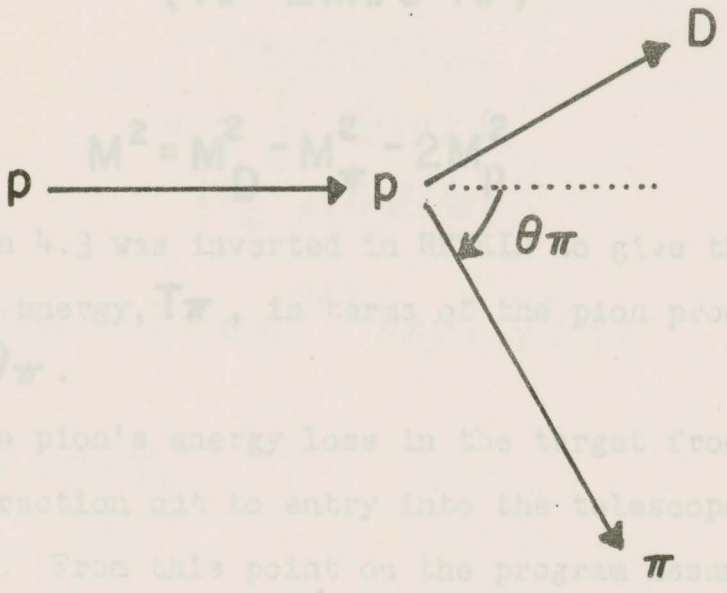

Fig.4.2 Schematic diagram of the reaction p(p,π)D

angle and pion energy, proton energy and the masses of the particles can be found. In particular:

$$\cos\theta_\pi = \frac{1}{2}\left(M^2c^4 - 2Mpc^2(Tp - T\pi + Mpc^2 - M\pi c^2)\right.$$
$$+2(TpT\pi + TpM\pi c^2 + T\pi Mpc^2$$
$$\left.+MpM\pi c^4)\right)\times(Tp^2 + 2Mpc^2\,Tp)^{-1/2}$$
$$\times(T\pi^2 + 2M\pi c^2\,T\pi)^{-1/2} \qquad (4.3)$$

where
$$M^2 = M_D^2 - M_\pi^2 - 2M_p^2$$

Equation 4.3 was inverted in REVKIN to give the pion kinetic energy, $T\pi$, in terms of the pion production angle, θ_π.

The pion's energy loss in the target from the point of interaction out to entry into the telescope was calculated. From this point on the program assumed normal REVMOC modelling and calculated multiple scattering through to counter S_4. The program also stored a spectrum of particles accepted into counter S_4, $N(\underline{p})$, as a function of initial pion momentum out of the target. The use of $N(\underline{p})$ in the calculation of the efficiency of detecting the pions is discussed in the following section.

4.1.2 Telescope Efficiency for Pions from $p(p,\pi)D$

To determine the number of pions which stop in counter S_4, the number of pions which fell inside the energy bite

including the energy straggle of the beam was calculated. The energy straggle is simply the fluctuation in energy loss for a given path length. The range straggle is the fluctuation in path length for a given energy loss and for these losses the straggle is assumed to be a gaussian distribution. If the average incident beam energy, T_b, is the average stopped pion energy, T_π, as shown in Fig.4.3, the efficiency of the telescope is given by:

$$\epsilon = \int_{(T_b - \Delta T/2)/\sigma_s}^{(T_b + \Delta T/2)/\sigma_s} \Phi(y)\, dy \qquad (4.4)$$

where $\Phi(y) = (2\pi\sigma_s)^{-1/2} \exp(-y^2/2)$

$$y = \frac{T - T_b}{\sigma_s}$$

σ_s is the root mean square energy straggle, and ΔT is the telescope energy bite.

From the definition of the error function equation 4.4 may be written:

$$\epsilon = \mathrm{erf}\,(\Delta T/(2 \cdot 2^{1/2}))$$

If the average beam energy is different from the mean telescope stopped pion energy, the telescope's energy bite is no

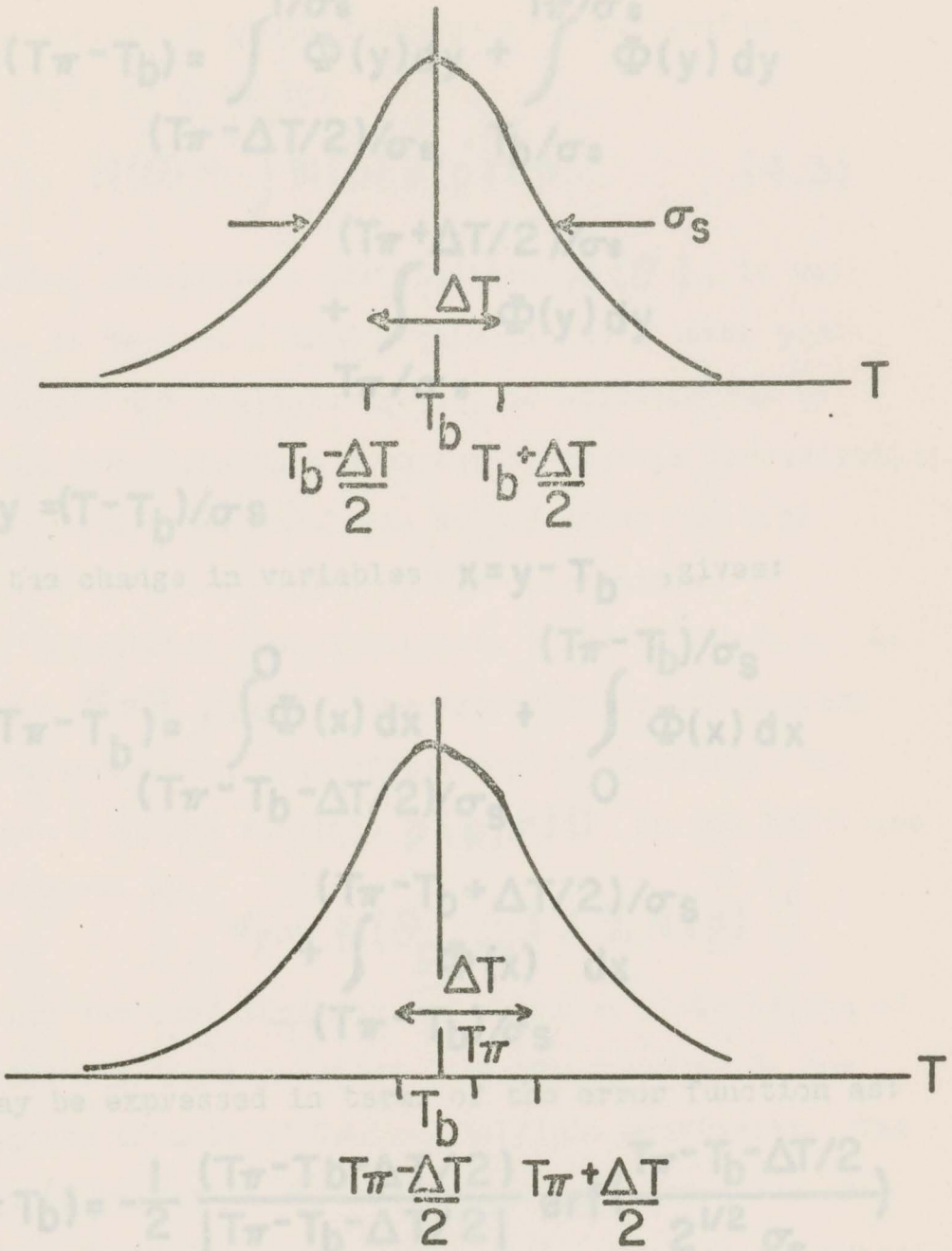

Fig.4.3 Curves which approximately represent the distributions of pions in energy when: (upper curve) the average incident beam energy T_b equals the average stopped pion energy, T_π; and (lower curve) when $T_b \neq T_\pi$. ΔT_π is the Energy bite of the Telescope.

longer symmetric about the beam energy, T_b, as shown in Fig.4.3. In this case the efficiency of the telescope is given by:

$$\epsilon(T_\pi - T_b) = \int_{(T_\pi - \Delta T/2)/\sigma_s}^{T/\sigma_s} \Phi(y)dy + \int_{T_b/\sigma_s}^{T_\pi/\sigma_s} \Phi(y)\,dy + \int_{T_\pi/\sigma_s}^{(T_\pi + \Delta T/2)/\sigma_s} \Phi(y)\,dy$$

where $y = (T - T_b)/\sigma_s$

Making the change in variables $x = y - T_b$, gives:

$$\epsilon(T_\pi - T_b) = \int_{(T_\pi - T_b - \Delta T/2)/\sigma_s}^{0} \Phi(x)\,dx + \int_{0}^{(T_\pi - T_b)/\sigma_s} \Phi(x)\,dx + \int_{(T_\pi - T_b)/\sigma_s}^{(T_\pi - T_b + \Delta T/2)/\sigma_s} \Phi(x)\,dx$$

which may be expressed in terms of the error function as:

$$\epsilon(T_\pi - T_b) = -\frac{1}{2}\frac{(T_\pi - T_b - \Delta T/2)}{|T_\pi - T_b - \Delta T/2|}\,\mathrm{erf}\left(\frac{T_\pi - T_b - \Delta T/2}{2^{1/2}\,\sigma_s}\right)$$

$$+\frac{1}{2}\frac{(T_\pi - T_b + \Delta T/2)}{|T_\pi - T_b + \Delta T/2|}\,\mathrm{erf}\left(\frac{T_\pi - T_b + \Delta T/2}{2^{1/2}\,\sigma_s}\right)$$

The values of σ_s for various mean telescope stopped pion energies have been calculated (Robertson 1976) and are given in Table 4.1.

The number of pions detected at a particular production angle is given by:

$$N(\theta) \propto \int N(p)\,\epsilon(p)\,dp \qquad (4.5)$$

In order to calculate a distribution, $N(\theta)$, it was possible to perform a REVKIN calculation at each production angle and evaluate Eq.4.5, or equivalently to shift the mean telescope momentum by amounts corresponding to a fixed angle and evaluate Eq.4.5 using the $N(p)$ distribution from a single REVKIN calculation. A typical calculated distribution is shown in Fig.4.4. At the angle $\theta = \theta_{peak}$, corresponding to the maximum in the distribution, the efficiency of detecting the pion beam from the reaction $p(p,\pi)D$ in the telescope bite is given by:

$$\epsilon_r = N(\theta_{peak}) / \Sigma N(p)$$

where the sum over $N(p)$ for the momentum distribution of particles which are accepted into the counter S_4 including the effects of Coulomb multiple scattering. The calculated values of ϵ_r corresponding to each run are listed in Table 4.2. The value of ϵ_r was not critically dependent upon σ_s. For a 1% deviation in σ_s there was approximately a 0.5% change in ϵ_r, reflecting the fact that the straggle is of the same order of magnitude as the energy bite of the telescope and the pion energy beam spread.

TABLE 4.1

R.M.S. ENERGY AND MOMENTUM STRAGGLE

MEAN STOPPED PION ENERGY $\bar{T}_\pi$ (MeV)	ROOT MEAN SQUARE ENERGY STRAGGLE σ_s (MeV)	MEAN STOPPED PION MOMENTUM $\bar{p}_\pi$ (MeV/c)	ROOT MEAN SQUARE MOMENTUM STRAGGLE σ_s (MeV/c)
52.0	0.93	131.0	1.35
75.0	1.32	163.0	1.72
102.0	1.78	197.0	2.17

(all values of σ_s calculated for copper)

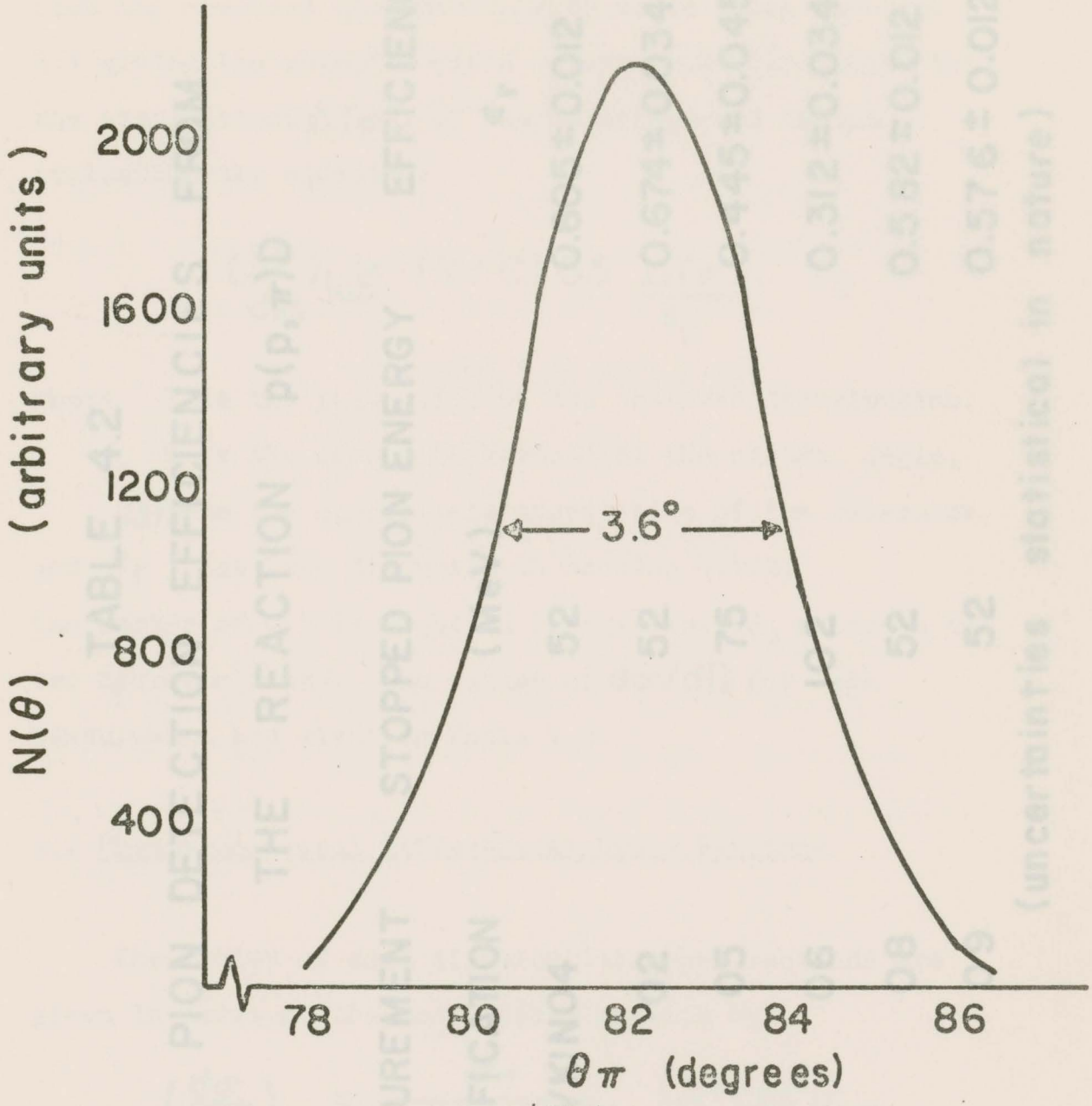

Fig.4.4 Calculated angular distribution of pions produced by 450 MeV protons in the reaction $p(p,\pi)D$.

TABLE 4.2

PION DETECTION EFFICIENCIES FROM THE REACTION $p(p,\pi)D$

MEASUREMENT IDENTIFICATION	STOPPED PION ENERGY (MeV)	EFFICIENCY ϵ_r
REVKIN04	52	0.605 ± 0.012
02	52	0.674 ± 0.034
05	75	0.445 ± 0.045
06	102	0.312 ± 0.034
08	52	0.582 ± 0.012
09	52	0.576 ± 0.012

(uncertainties statistical in nature)

4.1.3 Calculation of $d\sigma/d\Omega$ from the measured $d^2\sigma/dT_\pi d\Omega$

The differential cross section $d\sigma/d\Omega$ was calculated from the observed distributions by first using equation 3.1 giving the relative yield versus production angle into the energy bite, ΔT_π , of the telescope and second evaluating the equation:

$$\left(\frac{d\sigma}{d\Omega}\right)_{lab} = (Y - C)\, 0.5\, \frac{\Delta T_\pi}{\epsilon_r}$$

where Y is the peak value of the observed distribution,

C is the carbon background at the central angle,

ΔT_π is the appropriate energy bite of the telescope,

and ϵ_r has been discussed in section 4.1.2.

The factor of 0.5 is required because the CH_2 molecule has two hydrogen atoms. The values of $d\sigma/d\Omega$ for each measurement are given in Table 4.3.

4.2 Phenomenological Differential Cross Sections

The center of mass differential cross sections are given in terms of the total cross section by

$$\left(\frac{d\sigma}{d\Omega}\right)_{cm} = \frac{\sigma_T}{4\pi\left(A + \frac{1}{3} + \frac{B}{5}\right)} \left(A + \cos^2\theta_{cm} + B\cos^4\theta_{cm}\right)$$

The angular distribution parameters A and B have been most recently found to be (Axen et al 1976):

$$A = 0.31 \pm 0.04$$

$$B = 0.03 \pm 0.2$$

The total cross section has been expressed as:

$$\sigma_T = A_1\eta + A_2\eta^3 + A_3\eta^5$$

where η is the center of mass pion momentum in units of $m_\pi c$. The fitting parameters, based on a recent compilation of data (Spuller and Measday 1976) are:

$$A_1 = (0.186 \pm 0.010)\ mb$$

$$A_2 = (0.93 \pm 0.06)\ mb$$

$$A_3 = (-0.07 \pm 0.03)\ mb$$

The differential cross section were transformed to the lab frame and are presented in Table 4.3. The quoted uncertainties in these calculated cross sections have been made by adding the uncertainties of the fitting coefficients in quadrature.

TABLE 4.3

DIFFERENTIAL CROSS SECTION $d\sigma/d\Omega$ FOR THE REACTION $p(p,\pi)D$

MEASUREMENT IDENTIFICATION	STOPPED π ENERGY (MeV)	PION ANGLE θ_π	INCIDENT PROTON ENERGY (MeV)	$d\sigma/d\Omega$ (μb/sr) EXPERIMENT	THEORY
REVKIN04	52	97.0	500	127.2± 4.3	116 ± 12
02	52	96.0	500	120.0±6.7	116 ± 12
05	75	78.5	500	127 ± 18	112±11
06	102	64.0	500	119± 16	107 ± 11
08	52	82.0	450	76.3±3.8	78.8±7.9
09	52	64.0	400	49.9± 2.5	46.1±1.1

CHAPTER 5

DIFFERENTIAL CROSS SECTIONS FOR CARBON AND COPPER

5.1 Experimental Results

The differential cross sections for carbon are presented in Tables 5.1, 5.2 and 5.3. Graphs of the differential cross sections against pion energy for carbon are given in Fig.5.1 with the pion production angle as a parameter, and in Fig.5.2 with the proton energy as a parameter.

Each differential cross section is an average of all the runs at that proton energy and production angle throughout the experiment. For example the differential cross section for 53 MeV pions produced at an angle of 100° by 500 MeV protons on carbon, was observed to be: $(10.6 \pm 0.3)\mu$b/MeV·sr, $(10.4 \pm 0.3)\mu$b/MeV·sr, $(11.2 \pm 0.4)\mu$b/MeV·sr, and $(10.6 \pm 0.3)\mu$b/MeV·sr during three different shifts of the experiment. These four values were averaged to give $(10.7 \pm 0.2)\mu$b/MeV·sr. The agreement of these independent measurements is an indication of the internal consistancy of the experimental proceedures used.

The differential cross sections for copper are presented in Tables 5.4 and 5.5. Graphs of the differential cross sections against pion energy for copper are given in Fig.5.3 with the pion production angle as a parameter, and in Fig.5.4 with the proton energy as a parameter.

TABLE 5.1

DIFFERENTIAL CROSS SECTIONS FOR PIONS PRODUCED BY 500 MeV PROTONS INCIDENT ON CARBON

PION ENERGY (MeV)	$d^2\sigma/dT_\pi d\Omega$ ($\mu b/MeV \cdot sr$) $\theta_{\pi^+}=60°$	$\theta_{\pi^+}=100°$	$\theta_{\pi^+}=150°$
22.7		6.96±0.22	7.86±0.17
32.0	7.12±0.23	8.91±0.18	8.05±0.23
53.4	9.08±0.29	10.71±0.18	8.30±0.24
76.1	9.41±0.26	7.73±0.19	3.83±0.13
101.7	8.44±0.38	3.91±0.10	1.38±0.07

TABLE 5.2

DIFFERENTIAL CROSS SECTIONS FOR PIONS PRODUCED BY 450 MeV PROTONS INCIDENT ON CARBON

PION ENERGY	$d^2\sigma/dT_\pi d\Omega$ (μb/MeV·sr)		
(MeV)	$\theta_{\pi^+}=60°$	$\theta_{\pi^+}=100°$	$\theta_{\pi^+}=150°$
22.7	4.45±0.16	4.14±0.19	6.62±0.21
32.0	4.93±0.14	7.28±0.14	7.27±0.23
53.4	7.25±0.15	7.33±0.18	5.51±0.17
76.1	6.29±0.21	4.51±0.14	2.49±0.12
101.7	5.49±0.17	2.28±0.10	0.71±0.07

TABLE 5.3

DIFFERENTIAL CROSS SECTIONS FOR PIONS PRODUCED BY 400 MeV PROTONS INCIDENT ON CARBON

PION ENERGY (MeV)	$d^2\sigma/dT_\pi\, d\Omega$ (μb/MeV·sr) $\theta_{\pi^+}=60°$	$\theta_{\pi^+}=100°$	$\theta_{\pi^+}=150°$
22.7		4.79 ± 0.16	4.68 ± 0.17
32.0	3.65 ± 0.11 (T_π = 36.0 MeV)*	4.75 ± 0.12	5.25 ± 0.16
53.4	5.49 ± 0.18 (T_π = 56.4 MeV)	5.31 ± 0.16	3.49 ± 0.12
76.1	5.17 ± 0.16 (T_π = 78.7 MeV)	3.28 ± 0.15	1.46 ± 0.07
101.7	3.60 ± 0.14 (T_π = 104.0 MeV)	1.29 ± 0.05	0.43 ± 0.04

* due extra material in range telescope during these runs

TABLE 5.4

DIFFERENTIAL CROSS SECTIONS FOR PIONS PRODUCED BY 500 MeV PROTONS INCIDENT ON COPPER

PION ENERGY (MeV)	$d^2\sigma/dT_\pi d\Omega$ (μb/MeV·sr) $\theta_{\pi^+} = 60°$	$\theta_{\pi^+} = 100°$	$\theta_{\pi^+} = 150°$
22.7	17.0 ± 0.4	21.5 ± 0.7	20.8 ± 0.6
32.0	21.5 ± 0.7	26.1 ± 0.6	26.7 ± 0.9
53.4	26.0 ± 0.8	29.4 ± 0.7	25.1 ± 0.8
76.1	21.9 ± 0.7	19.6 ± 0.7	11.0 ± 0.7
101.7	18.1 ± 0.6	9.9 ± 0.4	4.6 ± 0.5

TABLE 5.5

DIFFERENTIAL CROSS SECTIONS FOR PIONS PRODUCED BY 450 MeV PROTONS INCIDENT ON COPPER

PION ENERGY (MeV)	$d^2\sigma/dT_\pi d\Omega$ (μb/MeV·sr) $\theta_{\pi^+}=60°$	$\theta_{\pi^+}=100°$	$\theta_{\pi^+}=150°$
22.7	13.3 ± 0.6	12.5 ± 0.6	15.1 ± 0.7
32.0	15.6 ± 0.6	17.6 ± 0.8	20.1 ± 0.9
53.4	16.2 ± 0.7	18.3 ± 0.8	17.7 ± 1.2
76.1	12.7 ± 0.6	9.2 ± 0.6	8.1 ± 0.9
101.7	10.7 ± 0.6	4.6 ± 0.5	2.5 ± 0.4

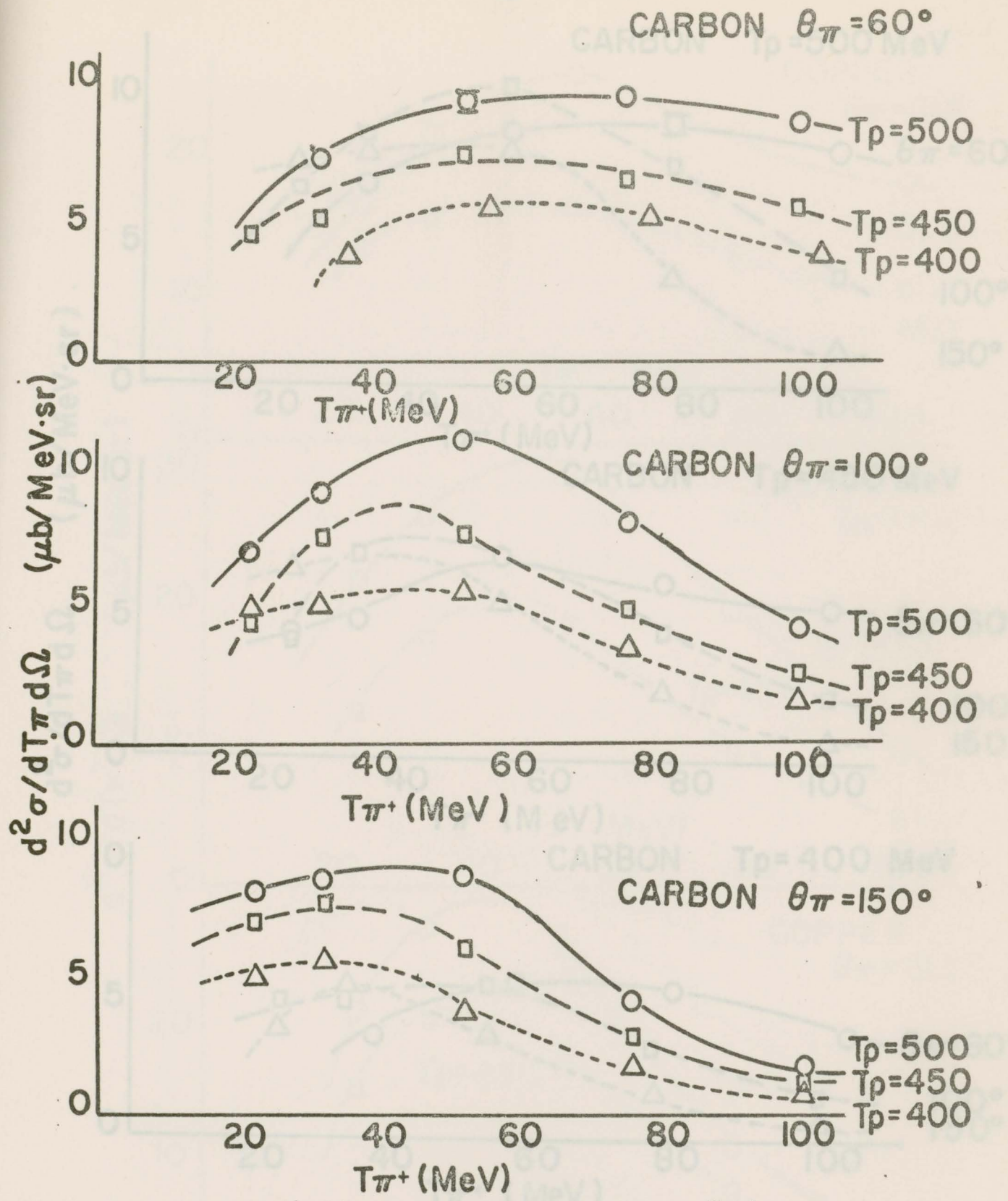

Fig.5.1 Differential Cross sections for pions produced by 400,450 and 500 MeV protons bombarding Carbon. The three plots are for pions produced at angles 60°, 100°, and 150°. Lines on these and following curves drawn to guide the eye.

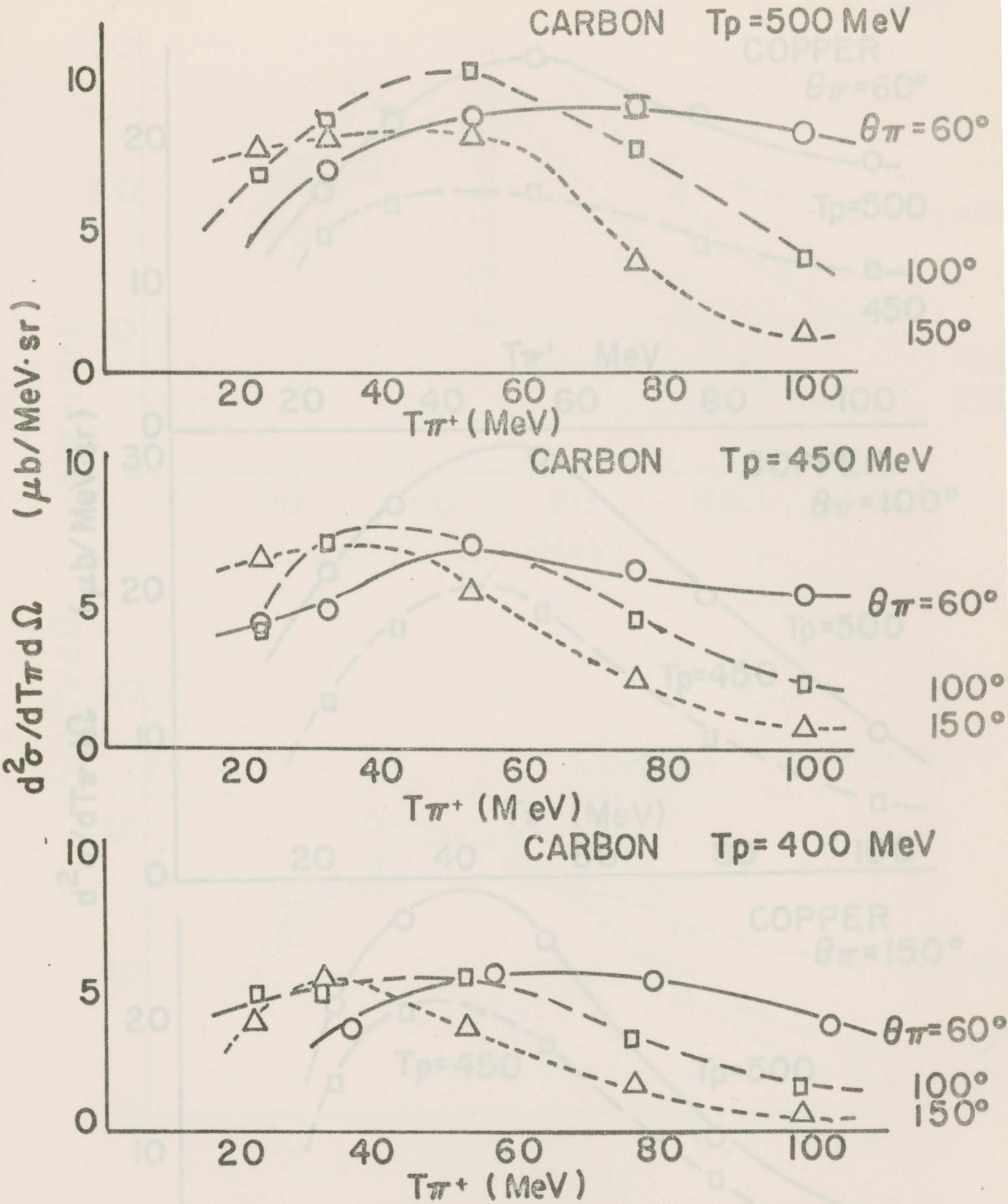

Fig. 5.2 Differential cross sections for pions produced at angles 60°, 100° and 150°. The three plots are for pions produced from 400, 450 and 500 MeV protons incident on car on.

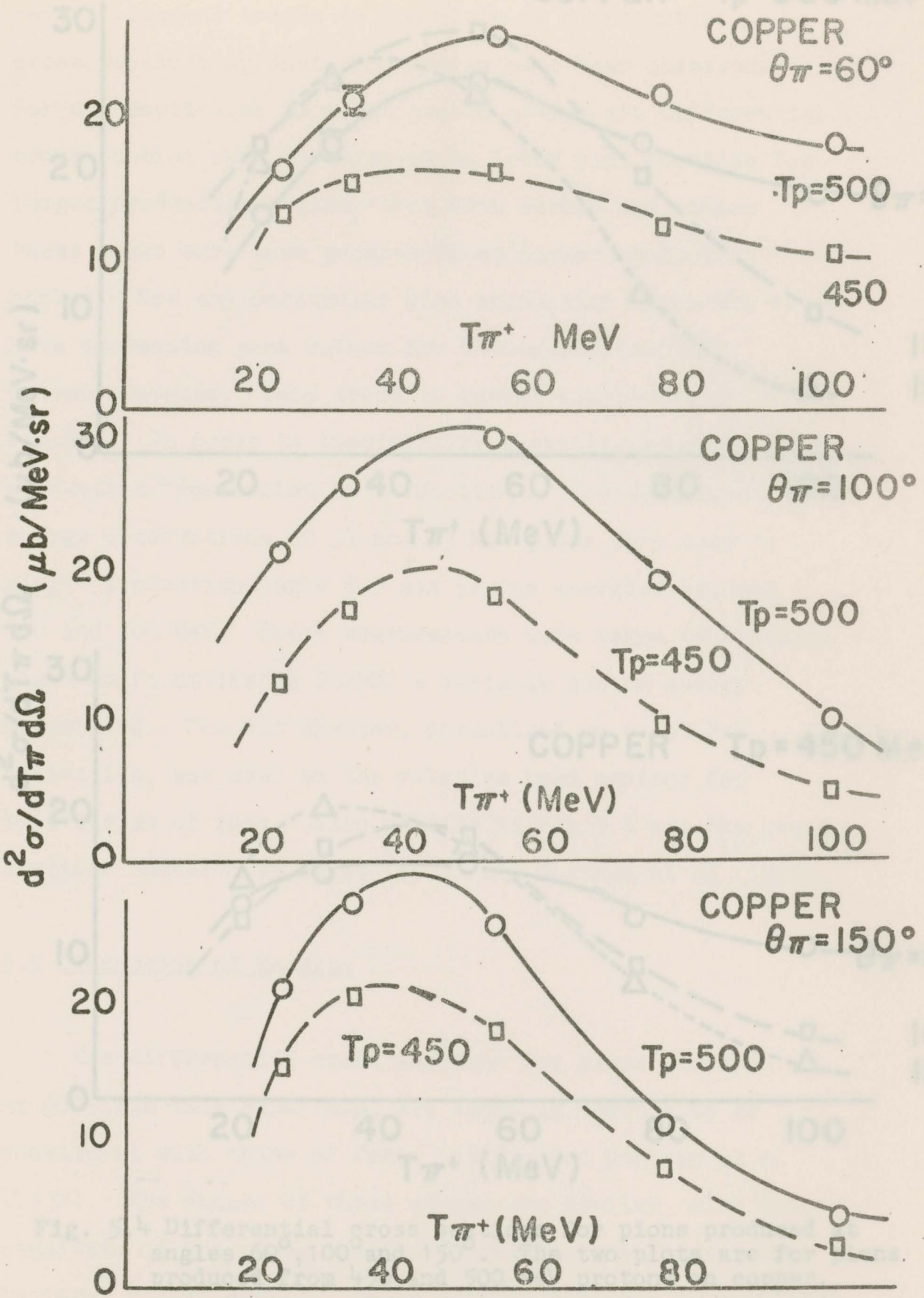

Fig. 5.3 Differential cross sections for pions produced by 450 and 500 MeV protons bombarding copper. The three plots are for pions produced at angles 60°, 100° and 150°.

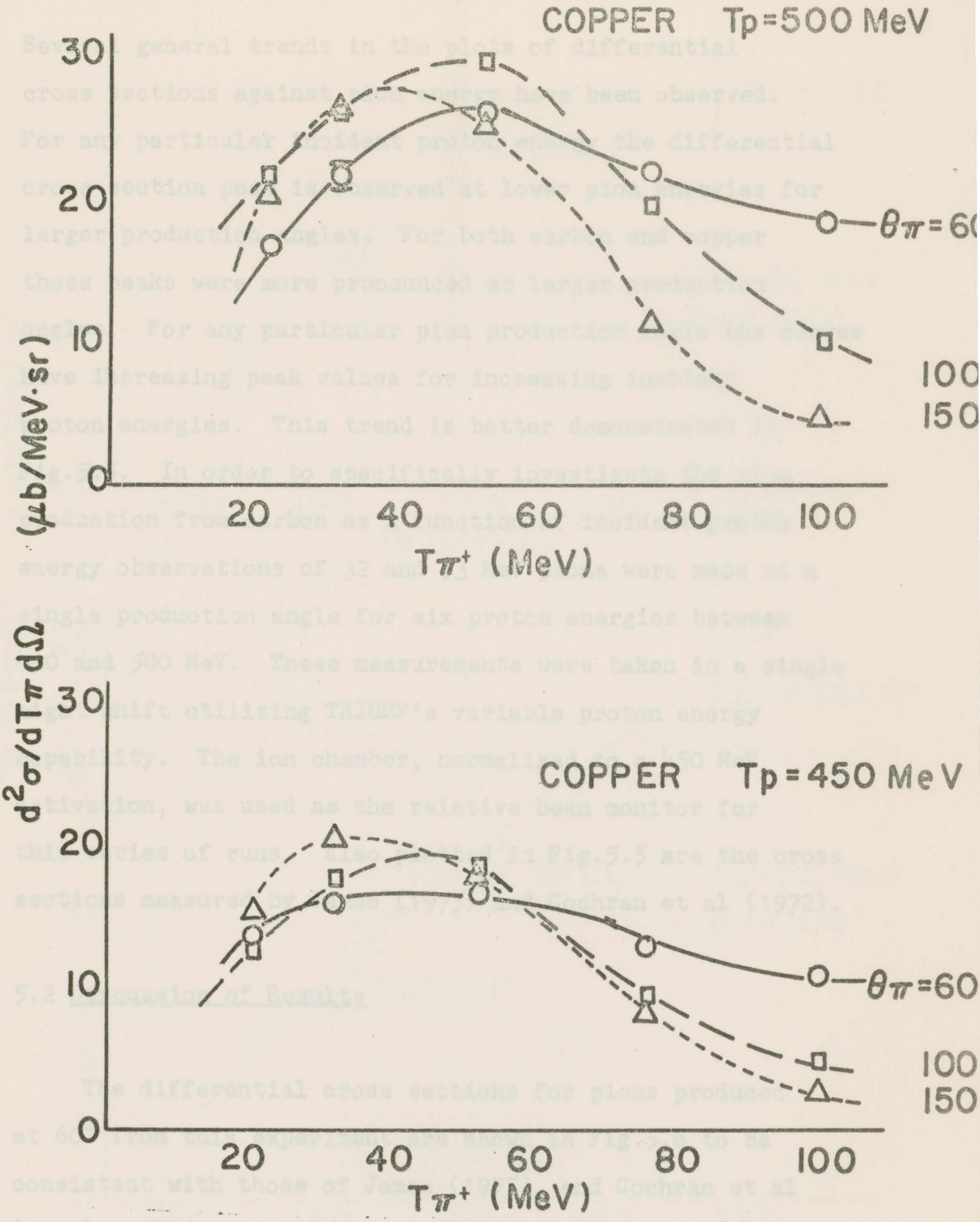

Fig. 5.4 Differential cross sections for pions produced at angles 60°, 100° and 150°. The two plots are for pions produced from 450 and 500 MeV protons on copper.

Several general trends in the plots of differential cross sections against pion energy have been observed. For any particular incident proton energy the differential cross section peak is observed at lower pion energies for larger production angles. For both carbon and copper these peaks were more pronounced at larger production angles. For any particular pion production angle the curves have increasing peak values for increasing incident proton energies. This trend is better demonstrated in Fig.5.5. In order to specifically investigate the pion production from carbon as a function of incident proton energy observations of 32 and 53 MeV pions were made at a single production angle for six proton energies between 400 and 500 MeV. These measurements were taken in a single night shift utilizing TRIUMF's variable proton energy capability. The ion chamber, normalized to a 450 MeV activation, was used as the relative beam monitor for this series of runs. Also plotted in Fig.5.5 are the cross sections measured by James (1975) and Cochran et al (1972).

5.2 Discussion of Results

The differential cross sections for pions produced at 60° from this experiment are shown in Fig.5.6 to be consistant with those of James (1975), and Cochran et al (1972). The shapes of these curves are similar, with the magnitude of the cross section increasing with increasing incident proton energy. These results disagree in magnitude

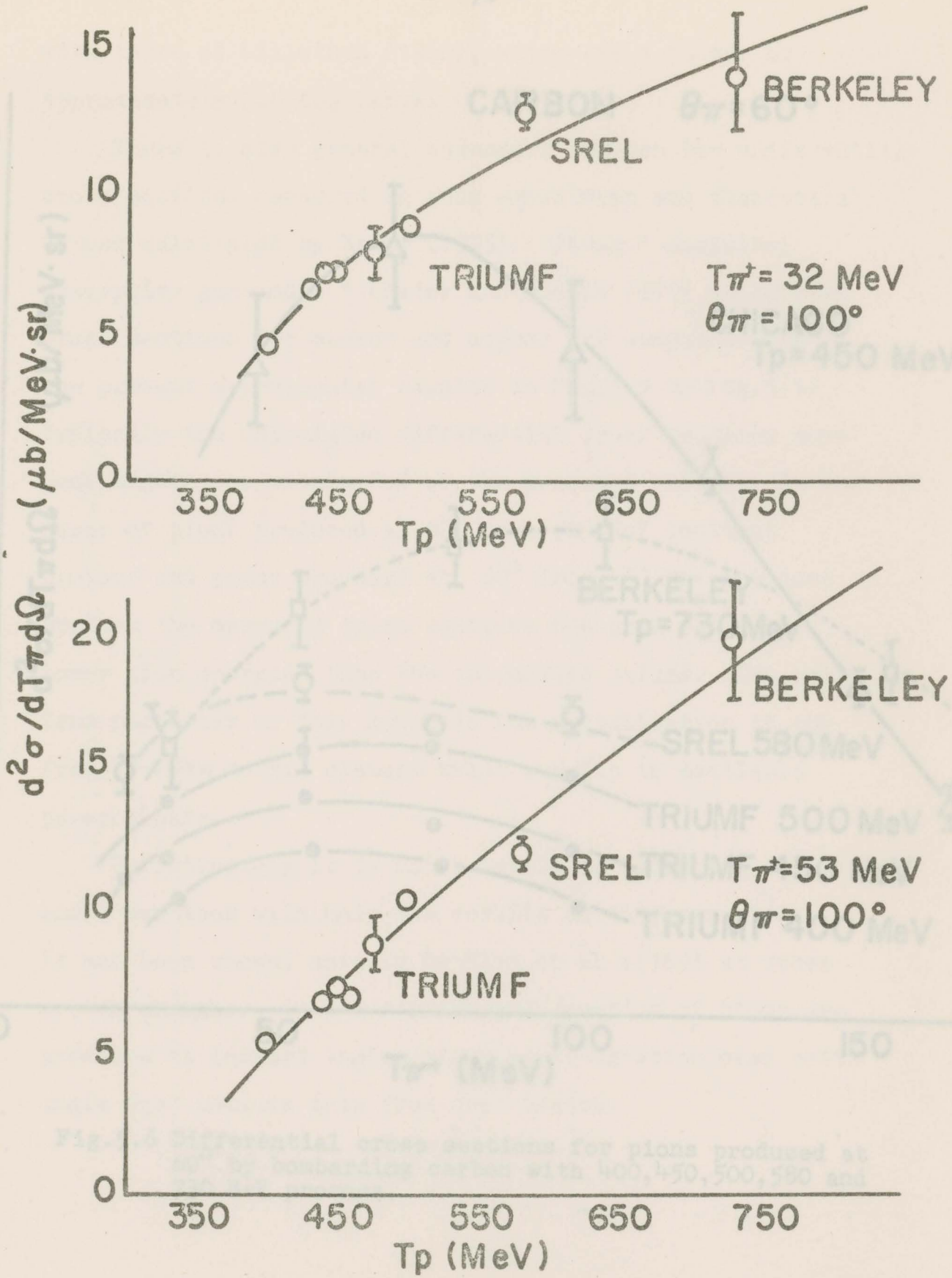

Fig. 5.5 Differential cross sections for 32 and 53 MeV pions produced at 100° from carbon as a function of proton energy between 350 and 700 MeV.

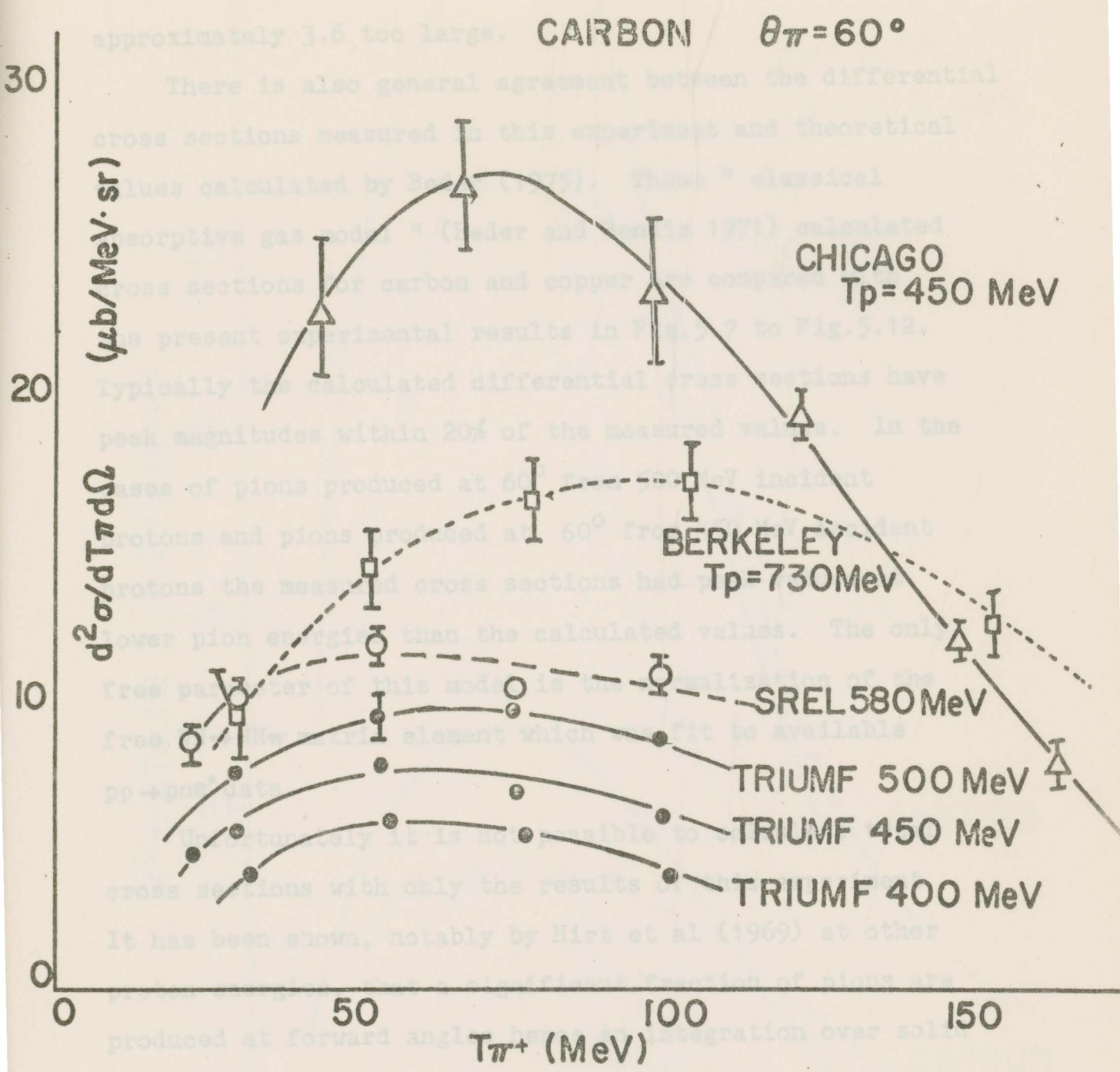

Fig.5.6 Differential cross sections for pions produced at 60° by bombarding carbon with 400,450,500,580 and 730 MeV protons.

with those of Lillethun (1962), which are a factor of approximately 3.6 too large.

There is also general agreement between the differential cross sections measured in this experiment and theoretical values calculated by Beder (1975). These " classical absorptive gas model " (Beder and Bendix 1971) calculated cross sections for carbon and copper are compared with the present experimental results in Fig.5.7 to Fig.5.12. Typically the calculated differential cross sections have peak magnitudes within 20% of the measured values. In the cases of pions produced at 60° from 500 MeV incident protons and pions produced at 60° from 450 MeV incident protons the measured cross sections had peak values at lower pion energies than the calculated values. The only free parameter of this model is the normalization of the free $NN \rightarrow NN\pi$ matrix element which was fit to available $pp \rightarrow pn\pi^{+}$ data.

Unfortunately it is not possible to calculate total cross sections with only the results of this experiment. It has been shown, notably by Hirt et al (1969) at other proton energies, that a significant fraction of pions are produced at forward angles hence an integration over solid angle must include data from that region.

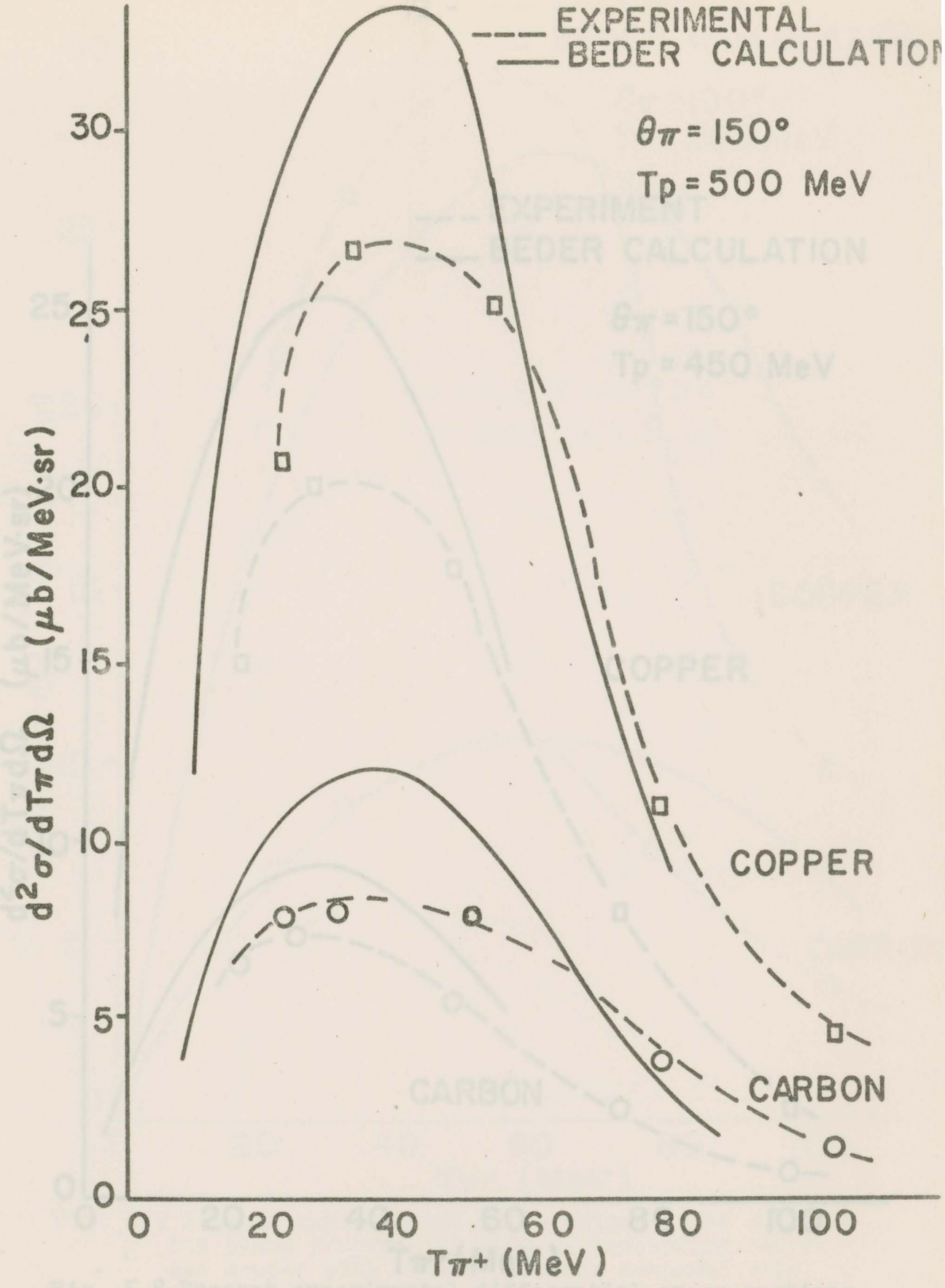

Fig. 5.7 Present experimental differential cross sections for pions produced at 150° by bombarding carbon and copper with 500 MeV protons compared with calculated results.

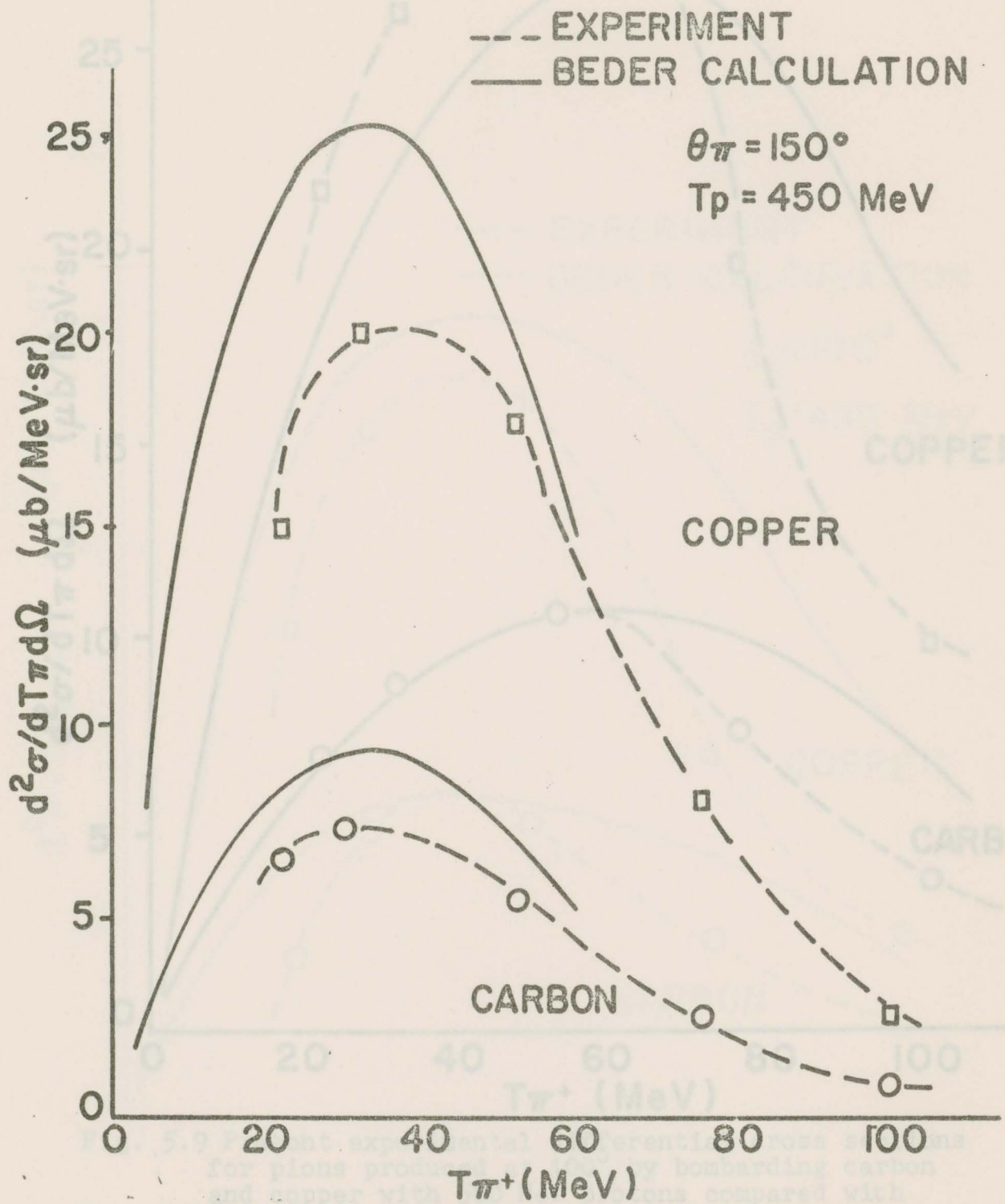

Fig. 5.8 Present experimental differential cross sections for pions produced at 150° by bombarding carbon and copper with 450 MeV protons compared with calculated results.

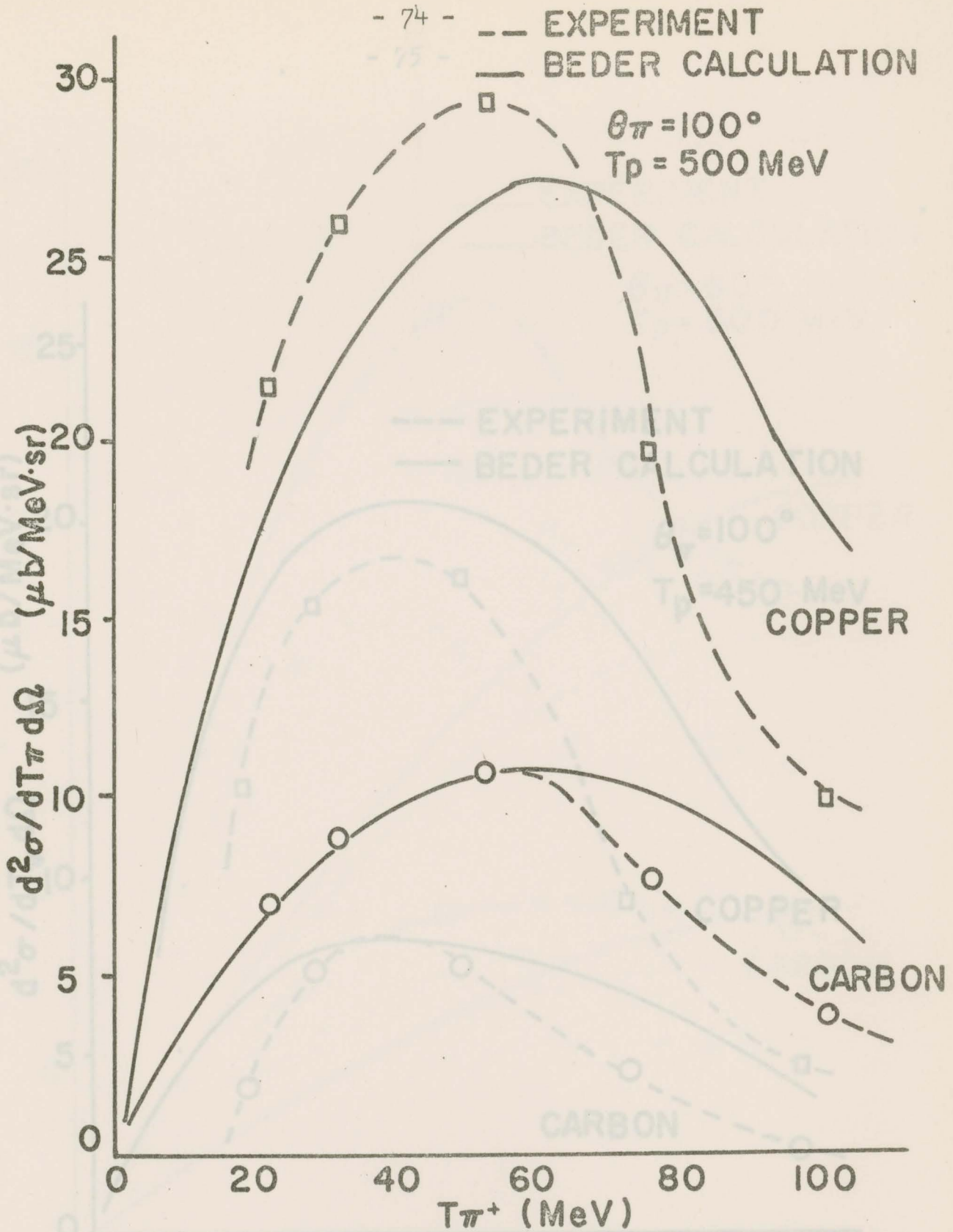

Fig. 5.9 Present experimental differential cross sections for pions produced at 100° by bombarding carbon and copper with 500 MeV protons compared with calculated results.

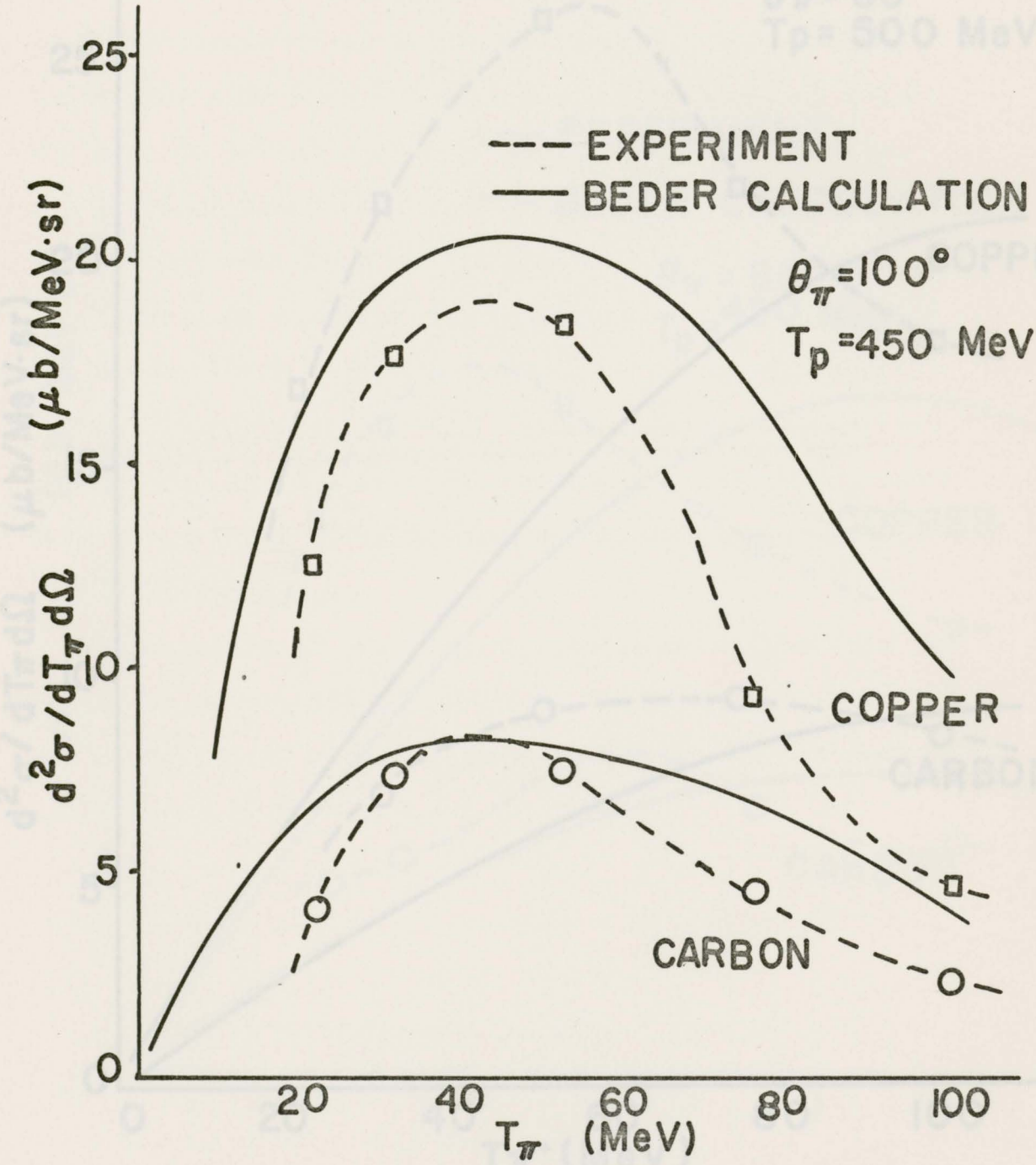

Fig.5.10 Present experimental results for pions produced at 100° by bombarding carbon and copper with 450 MeV protons compared with calculated results.

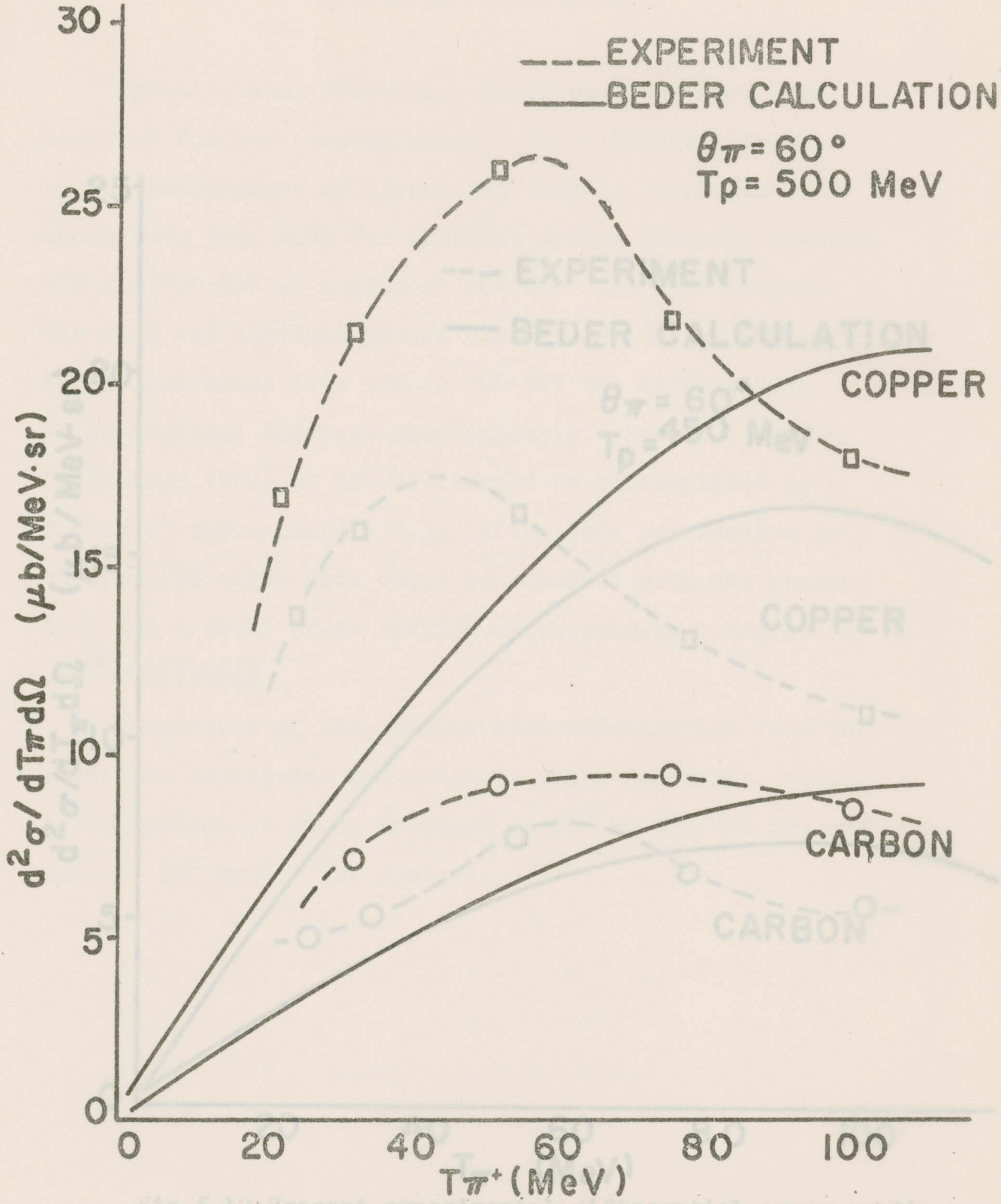

Fig. 5.11 Present experimental differential cross sections for pions produced at 60° by bombarding carbon and copper with 500 MeV protons compared with calculated results.

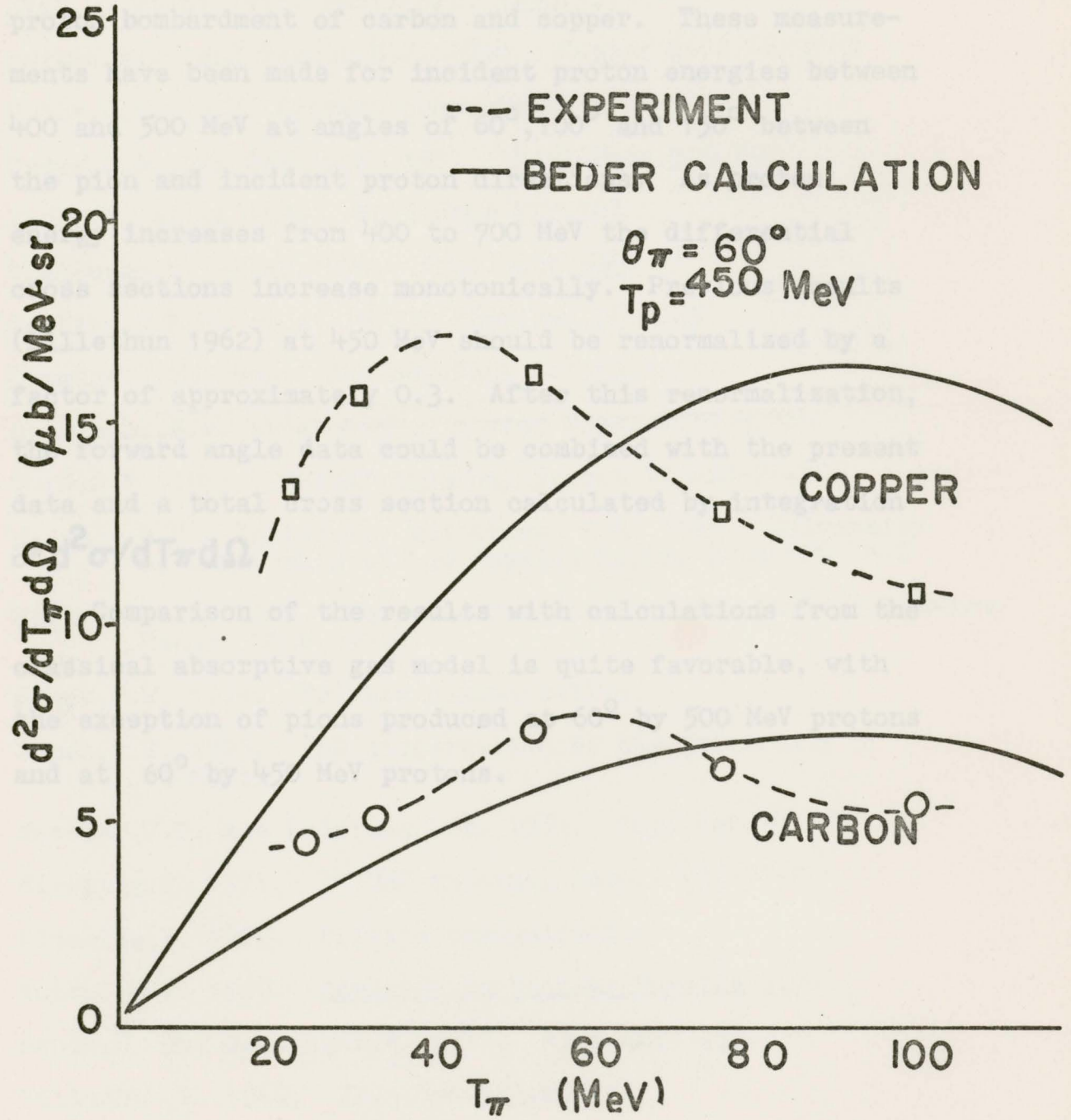

Fig.5.12 Present experimental differential cross sections for pions produced at 60° by bombarding carbon and copper with 450 MeV protons compared with calculated results.

CHAPTER 6

SUMMARY AND CONCLUSIONS

Positive pion production cross sections have been measured for low energy pions (20 - 100 MeV) from proton bombardment of carbon and copper. These measurements have been made for incident proton energies between 400 and 500 MeV at angles of 60°, 100° and 150° between the pion and incident proton directions. As proton energy increases from 400 to 700 MeV the differential cross sections increase monotonically. Previous results (Lillethun 1962) at 450 MeV should be renormalized by a factor of approximately 0.3. After this renormalization, the forward angle data could be combined with the present data and a total cross section calculated by integration of $d^2\sigma/dT_\pi d\Omega$.

Comparison of the results with calculations from the classical absorptive gas model is quite favorable, with the exception of pions produced at 60° by 500 MeV protons and at 60° by 450 MeV protons.

REFERENCES

Ajzenberg-Selove,F. and Lauritsen,T. 1968. Nucl.Phys.A114,22

Anspach,S.C. et al 1965. Natl.Bur.Stand.,Misc.Publ.260-9

Axen,D. et al 1976. Nucl.Phys. A256,387

Barkas,W.H. and Berger,M.J. 1964. Report NASA SP-3013

Beder,D.S. 1975. Private communication.

Beder,D.S. and Bendix,P. 1971. Nucl.Phys.B26,597

Binon,F. et al 1970. Nucl.Phys.B17,168

Chaloupka,V. et al 1974. Phys.Lett.50B

Cochran,D.R.F. et al 1972. Phys.Rev.D6,3085

Cumming,J.B. 1963. Ann.Rev.Nucl.Sci.13,261

Dzhelepov,V.P. et al 1957. Soviet Phys. JETP.4,864

Gurd,D.P. 1971. TRIUMF internal report TRI-DN-71-40

Haddock,R.P., Zeller,M., and Crowe, K.M. 1964. University of California at Los Angeles Report UCLA-MPG 64-2

Hirt,W. et al 1969. European Organization for Nuclear Research Report CERN 69-24

James,P.W. 1974. Private communication.

James,P.W. 1975. PhD dissertation at the University of Victoria

Kessler,J.O. and Lederman,L.M. 1954. Phys.Rev.94,689

Kitching,P. 1971. TRIUMF internal report TRI-71-2

Kitching,P. 1975. Private communication.

Koltun,D.S. 1969. Advances in Nuclear Physics 3,71

Leutz,H. and Wenninger,H. 1967. Nucl.Phys.A99,55

Lillethun,E. 1962. Phys.Rev.123,665

Meshkovskii,A.G., Shalamov,I.I., and Shebanov, V.A. 1958. Soviet Phys. JETP.34,987

Molière,G. 1959. Z.Physik.156,318

Olin,A. 1975. Private communication.

Robertson,L.P. 1976. Private communication.

Spuller,J and Measday,D.F. preprint of 'On the s-wave production of pions in p(p,π)D' submitted to Phys.Rev.D.

Stetz,A.W. 1975. Private communication.

Williams,A. 1964. Nucl.Phys.52,324

Vereschagin,A.N. et al 1968. Isz.Akad.Nauk.32,623

APPENDIX A

DATA ACQUISITION PROGRAM

The data acquistion program served to record all the experimental parameters at the start of each run and to read and clear the information recorded in CAMAC scalars. A preliminary calculation of cross section was performed for each run. The program was written in TRIUMF BASIC (Gurd 1971) which is the normal BASIC language plus a series of assembler language subroutines for CAMAC operations which are accessed by a normal BASIC CALL statement. A simplified flow chart for the program is given in Fig.A.1. A copy of the program is reproduced on the following three pages.

From statements 7 to 960 is the control section of the program. In an interactive mode the user types in information such as run identification, target parameters, proton and pion energies and pion production angle. Once directed to do so in the control section, the program read all the information in the CAMAC units by executing statements 1100 to 1210. The user would then decide to execute statements 2000 to 3099, calculating a preliminary cross section and obtaining hard copy of all CAMAC information, or to execute statements 5000 to 9012 which would clear all CAMAC units in preparation for the next run.

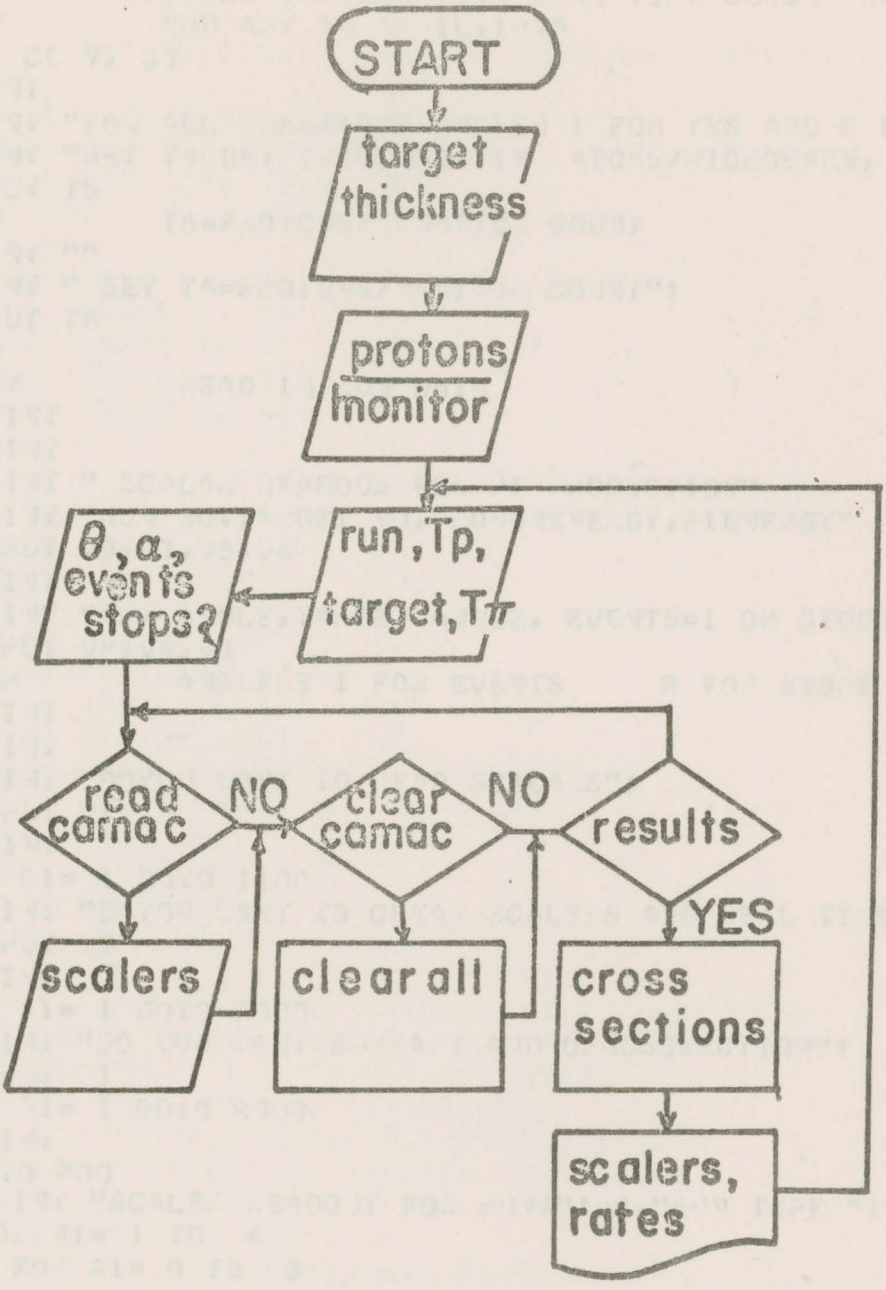

Fig. A.I FLOWCHART FOR DATA ACQUISITION PROGRAM

```
7  REM    JULY 11 VERSION WITH 12-FOLD SCALAR
8  REM     RE-RETYPED ON 9 JULY 75
9  REM       RETYPED VERSION WITH REAL TIME CLOCK  22 MAY 75
10 REM        MOD AT 15 APRIL,1975
20 DIM C[ 7, 5]
41 PRINT
50 PRINT "FOR ALL QUESTIONS ANSWER 1 FOR YES AND 0 FOR NO"
60 PRINT "SET TARGET THICKNESS IN  ATOMS/MICROBARN, T5=";
61 INPUT T5
65 REM          T6=PROTONS/ MONITOR COUNT
69 PRINT ""
70 PRINT " SET T6=PROTONS/MONITOR COUNT";
75 INPUT T6
99 REM
100 REM         READ IN RUN DATA
108 PRINT
109 PRINT
110 PRINT " SCALAR READOUS FOR PI PRODUCTION"
800 PRINT "RUN NO.TARGET NO,PHONONENERGY,PIENERGY"
801 INPUT V9,V7,V5,V6
802 PRINT
803 PRINT "ARM ANGLE,TARGET ANGLE, EVENTS=1 OR STOPS=2"
804 INPUT V8,V4,V3
825 REM          ANSWERE 1 FOR EVENTS     2 FOR STOPS -RUN
900 PRINT
911 PRINT
913 PRINT "DOYOU WANT TO READ SCALARS";
921 INPUT C1
922 PRINT
925 IF C1= 1 GOTO 1100
930 PRINT "DOYOU WANT TO CLEAR SCALERS AND REAL TIME CLOCK";
931 INPUT C1
932 PRINT
933 IF C1= 1 GOTO 9000
940 PRINT "DO YOU WANT SUMMARY AND CROSSSECTION";
941 INPUT C1
942 IF C1= 1 GOTO 2000
943 PRINT
960 GOTO 900
1100  PRINT "SCALER READOUT FOR RUN#";V9,"RUN TYPE ";V3
1110  FOR N1= 1 TO  4
1111    FOR A1= 0 TO  3
1125      CALL  1, 0,N1,A1, 0,D1,E1
1130      LET C[N1,A1]=D1
1135    NEXT A1
1140    PRINT N1,C[N1, 0],C[N1, 1],C[N1, 2],C[N1, 3]
1145  NEXT N1
1150  LET N1= 3
1155  GOTO 1200
1160  CALL  1, 0,N1,A1, 0,D1,E1
1165  LET N2=N1+ INT (A1/ 4)
1170  LET A2=A1-(N2-N1)* 4
```

```
1170  LET A2=A1-(N2-N1)* 4
1175  LET D1=C[N2,A2]
1176  NEXT A1
1180  FOR N2= 3 TO  5
1185    PRINT N2,C[N2, 0],C[N2, 1],C[N2, 2],C[N2, 3]
1190  NEXT N2
1200  PRINT "END OF SCALAR LEADS"
1205  LET D2=C[ 4, 0]
1206  PRINT " REAL TIME  ";D2/ 60
1207  PRINT
1209  PRINT
1210  GOTO 930
2000  LET S6=C[ 1, 0]
2001  LET S7=C[ 1, 1]
2002  LET S8=C[ 1, 2]
2003  LET S9=C[ 1, 3]
2004  PRINT
2006  PRINT " IN #";V0," CPU TYPE ";V3
2010  PRINT "STO-S ";S6;"EVENTS ";S7
2020  LET A0=C[ 4, 0]
2022  LET A3=S7-A0-1
2030  LET A1=C[ 4, 1]
2040  LET T1= 24.16
2041  LET V1=C[ 2, 1]
2042  LET V2=C[ 3, 0]
2043  LET V3=C[ 3, 1]
2044  LET V4=C[ 3, 2]
2045  LET V5=V1-V2-V3-V4
2046  LET A6=S6/V5
2047  LET A7=S7/V5
2048  LET V7=C[ 2, 2]
2049  LET V8=C[ 2, 3]
2050  PRINT "REAL MONITOR";V5;"  V1 ";V1
2051  PRINT "V1(1) ";V2;"V1(2) ";V3;" V1(3) ";V4
2052  PRINT " STOPS/MONITOR ";A6;" EVENTS/MONITOR ";A7
2053  PRINT "ALIA I C ";V8;" SEM ";V7
2060  PRINT "(SI)D";A0;"(1)234=5";A1
2070  PRINT "MON/SEC";V5/V7;"MON/I C";V5/V8
2073  PRINT "S12";C[ 4, 2];"S13 ";C[ 4, 3]
2090  LET A5=C[ 2, 0]
2100  PRINT "COINC RATES'"
2101  PRINT "1-2 ";S9;"1-(2)  ";A5
3000  LET I1= INT (V6/ 10)
3002  LET G[ 3]= .000685
3003  LET G[ 5]= .00068
3004  LET G[ 7]= .0005
3005  LET G[ 10]= .000419
3006  LET G[ 2]= .000693
3010  LET A4=E7* COS (V4/ 57.3)/G[I1]
3015  LET A8=A3/(T5*T6)
3020  PRINT " "
3025  PRINT "       CROSS SECTION ",A8
```

```
3040  LET D1=65/CL A, 0]* 60*16* 1.6E-10
3050  PRINT " BEAM CURRENT ";D1;"  MA"
3060  PRINT
3099  GOTO 110
5000  REM     REAL TIME CLOCK NOT USED. PULSES 60CPS SCALED
5010  PRINT "SCALING CLOCK IS CLEARED"
5012  GOTO 9000
9000  FOR M1= 1 TO  4
9001    FOR A1= 0 TO  3
9004      CALL  1, 0,M1,A1, 2,D2,E1
9005    NEXT A1
9006  NEXT M1
9007  GOTO 940
9008  CALL  1, 0, 3,A1, 2,D2,E1
9009  NEXT A1
9010  PRINT "SCALERS CLEARED "
9011  PRINT
9012  GOTO 940
9999  END
```

APPENDIX B

CALCULATION OF INCIDENT PROTON INTENSITY

The $^{12}C(p,pn)^{11}C$ activation technique has been summarized by James (1975), who demonstrated that the number of protons incident on a ^{12}C foil in bombarding time T_o is given by:

$$I = \frac{R}{2\epsilon\Omega} \frac{\lambda}{\rho\sigma} \frac{T_o}{1-\exp(\lambda T_o)} \frac{T}{1-\exp(-\lambda T)} \qquad (B.1)$$

where R is the ^{11}C decay rate measured at time T,

$\epsilon\Omega$ is the efficiency and solid angle product discussed in section 2.5,

λ is the inverse of the mean lifetime of the ^{11}C decay,

ρ is the number of ^{12}C nuclei per unit area of the target,

and σ is the $^{12}C(p,pn)^{11}C$ activation cross section (Cumming 1963)

The ASPEC (Olin 1975) program is a general utility program for utilizing data stored on magnetic tape by the pulse height analyzer. This program was used to read the ^{11}C decay spectra and calculate the incident proton flux using the subroutine INTEN which is described below.

For a typical activation up to ninety 200 second spectra were recorded. For each spectrum the program would record the number of counts in the 0.51 MeV gamma peak per unit time (ARSAV), and the time at which the

spectrum was recorded with respect to the beginning of the bombardment (T). The program required values of λ, T_o, $\epsilon\Omega$, ρ and σ for each calculation. From Fig.2.11, the values of σ are 30.8 ± 1.5 mb, 31.7 ± 1.6mb, and 32.6 ± 1.6 mb for proton energies 500,450 and 400 MeV respectively.

For bombarding times less than five minutes, equation B.1 has been written:

$$\text{BEAM} = I = \frac{R}{T_o} \frac{1}{2\epsilon\Omega} \frac{1}{\rho\sigma} \frac{\exp(\lambda(T-T_o))}{1-\exp(-\lambda T_o)} \qquad (B.2)$$

In the subroutine INTEN, the program evaluated equation B.2 for each of a user specified series of spectra and averaged them for a final value. The series of spectra were chosen which involved intensities of ^{11}C decays of the same magnitude as the intensity of ^{22}Na decays which were used to determine $\epsilon\Omega$.

A simplified flowchart of INTEN is given in Fig.B.1 and a copy of the program is presented on the following page.

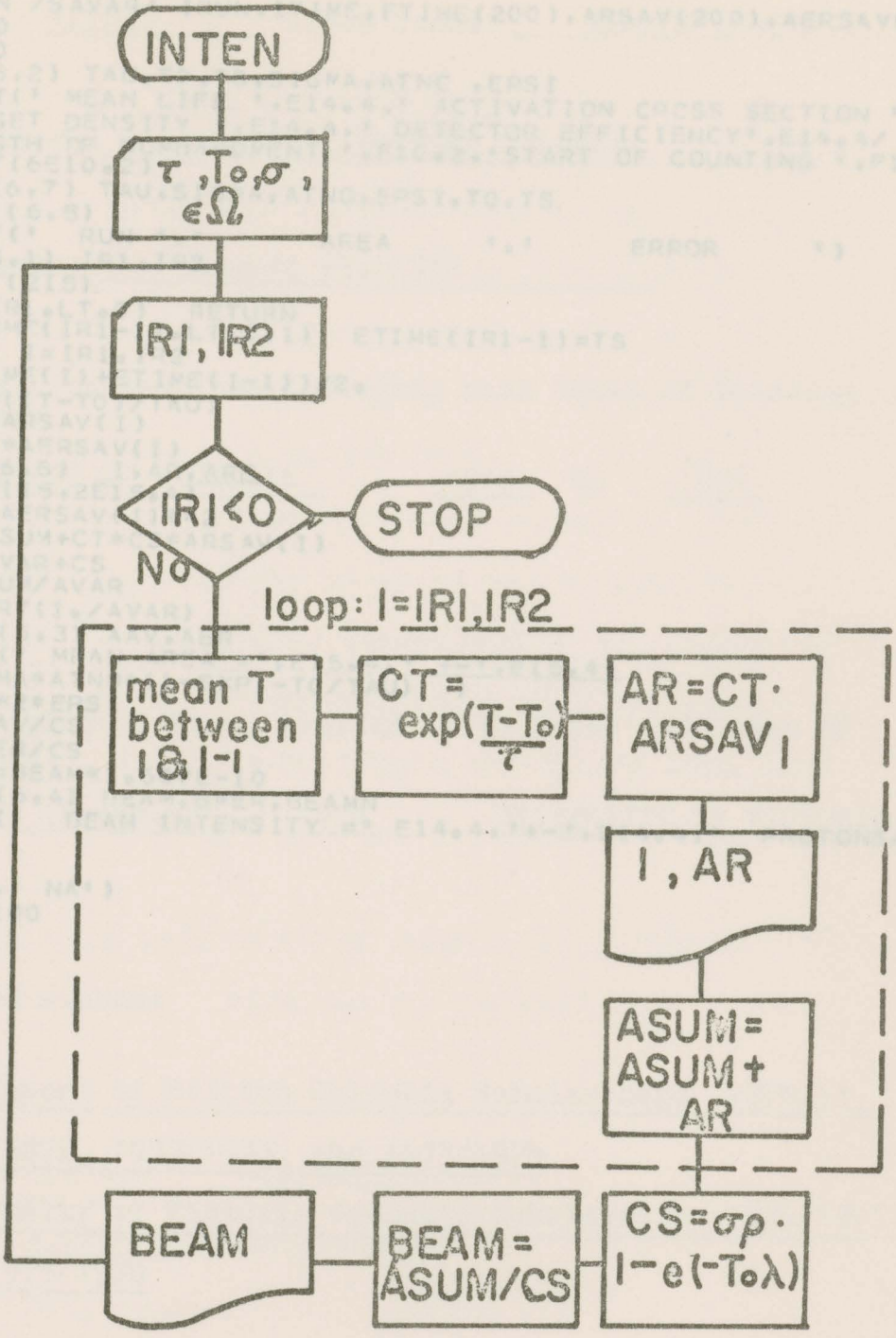

FIG. B.1 FLOWCHART FOR ROUTINE INTEN.

INTEN

```
      SUBROUTINE INTEN
      COMMON /SAVAR/ IRUN,ITIME,ETIME(200),ARSAV(200),AERSAV(200)
      ASUM=0
      AVAR=0
      READ(5,2) TAU,TO,TS,SIGMA,ATNO ,EPSI
    7 FORMAT(' MEAN LIFE ',E14.4,' ACTIVATION CROSS SECTION ',E14.4/
     1' TARGET DENSITY ',E14.4,' DETECTOR EFFICIENCY',E14.4/
     2' LENGTH OF BOMBARDMENT ',F10.2,'START OF COUNTING ',F10.2)
    2 FORMAT(6E10.2)
      WRITE(6,7) TAU,SIGMA,ATNO,EPSI,TO,TS
      WRITE (6,5)
    5 FORMAT('  RUN ','       AREA      ','      ERROR      ')
  100 READ(5,1) IR1,IR2
    1 FORMAT(2I5)
      IF (IR1.LT.0)  RETURN
      IF(ETIME(IR1-1).LT.0.1)  ETIME(IR1-1)=TS
      DO 200 I=IR1,IR2
      T=(ETIME(I)+ETIME(I-1))/2.
      CT=EXP((T-TO)/TAU)
      AR=CT*ARSAV(I)
      ARE=CT*AERSAV(I)
      WRITE(6,6)  I,AR,ARE
    6 FORMAT(I5,2E15.4)
      CS=1./AERSAV(I)**2
      ASUM=ASUM+CT*CS*ARSAV(I)
  200 AVAR=AVAR+CS
 1000 AAV=ASUM/AVAR
      AER=SQRT(1./AVAR)
      WRITE (6,3) AAV,AER
    3 FORMAT(' MEAN AREA =',E15.4,' +-',E15.4)
      CS=SIGMA*ATNO*(1-EXP(-TO/TAU)   )
       CS=CS*2*EPSI
      BEAM=AAV/CS
      BMER=AER/CS
       BEAMN=BEAM*1.602E-10
       WRITE(6,4) BEAM,BMER,BEAMN
    4 FORMAT('  BEAM INTENSITY =' E14.4,'+-',E14.4,'  PROTONS/SEC  ='
     1 F10.3,' NA')
      GO TO 100
      END
```

VITA

Surname: MATHIE Given Names: EDWARD LAWRENCE

Place of Birth: KELOWNA, BRITISH COLUMBIA

Date of Birth: August 24, 1952

Educational Institutions Attended, with Dates of Entering and Leaving:

UNIVERSITY OF VICTORIA 1970 to 1976

Degrees, Diplomas, Etc., Awarded, with Dates and Names of Institutions:

B.Sc. (Honours) 1974 UNIVERSITY OF VICTORIA

Honours and Awards:

Government of British Columbia Scholarships 1970/71, 1971/1972, 1972/1973, and 1973/1974

University of Victoria Graduate Scholarships 1974/1975, and 1975/1976

PARTIAL COPYRIGHT LICENSE

I hereby grant the right to lend my thesis (the title of which is shown below) to users of the University of Victoria Library, and to make single copies only for such users or in response to a request from the library of any other university, or similar institution, on its behalf or for one of its users. I further agree that permission for extensive copying of this thesis for scholarly purposes may be granted by me or a member of the University designated by me. It is understood that copying or publication of this thesis for financial gain shall not be allowed without my written permission.

LOW ENERGY PION PRODUCTION BY PROTONS WITH INCIDENT ENERGIES FROM 400 TO 500 MeV

Author [redacted]

EDWARD LAWRENCE MATHIE

MAY, 1976